Inferring late-Holocene climate in the Ecuadorian Andes using a chironomid-based temperature inference model

Frazer Matthews-Bird[1&2], matthewsbirdf@fit.edu

Stephen J. Brooks[3], S.Brooks@nhm.ac.uk

Philip B. Holden[1], philip.holden@open.ac.uk

Encarni Montoya[1], encarni.montoya@open.ac.uk

William D. Gosling[1, 4], W.D.Gosling@uva.nl

[1]Department of Earth, Environment & Ecosystems, The Open University, Walton Hall, Milton Keynes, MK7 6AA, UK.

[2] Biological Sciences, Florida Institute of Technology, 150 West University Boulevard, Melbourne, FL 32901, USA

[3]Department of Life Sciences, Natural History Museum, Cromwell Road, London SW7 5BD, UK.

[4]Palaeoecology & Landscape Ecology, Institute for Biodiversity & Ecosystem Dynamics, University of Amsterdam, P.O. Box 94248, 1090 GE Amsterdam, The Netherlands

Corresponding author: Frazer Matthews-Bird

Key words: Bayesian, weighted-averaging, transfer function, chironomids, Holocene climate change, Ecuador

1. Introduction

Holocene climate variability (11.7 kcal yrs BP – present) offers the most recent opportunity to parameterise climate and ecosystem responses to natural forcing under current boundary conditions in the absence of intense anthropogenic activity (Mayewski *et al*., 2004; Oldfield and Steffen, 2014). Furthermore, quantitative estimates of past climate over long time scales (>1000 yrs) are vital to improving the reliability of modelling and prediction of present and future climate variability (Mayewski *et al*., 2004). The spatial distribution of palaeoclimate records, however, is currently uneven around the world. Quantitative reconstructions of past climate are common from mid- to high- latitudes of both hemispheres but data is much scarcer from low-latitude (tropical) regions (Jansen *et al.*, 2007). Tropical climate is the dominant driver of atmospheric circulation (Ivanochko *et al., 2005)* and the source of intermittent phenomena, such as the El Niño Southern Oscillation (ENSO), which has a global influence on climate (Collins *et al*., 2010). Quantitative estimates of past climate from the low latitude tropics, therefore, are crucial for investigating not only regional climate processes, but also teleconnections on long timescales (>1000 years) (Garreaud *et al.*, 2009; Jomelli *et al*., 2009; Vuille *et al*., 2000). Here we develop the first chironomid-based temperature inference model for tropical South America. The model is applied to a Holocene lake sediment sequence to generate a chironomid-inferred temperature reconstruction from the tropical East Andean flank.

Chironomidae (non-biting midges) is a family of two-winged aquatic insects of the order Diptera. The family is globally distributed and one of the most diverse within aquatic ecosystems (Armitage *et al*., 1995). Many species are stenotopic, and their short life-cycles and ability to colonise favourable regions quickly means the insects are extremely sensitive to environmental change (Pinder, 1986). The head capsules of chironomid larvae are well preserved in lake sediments and have been used extensively as palaeoecological proxies (Brooks, 2006; Walker and Cwynar, 2006). Chironomid-based temperature inference models, derived from modern calibration data sets, have been applied across North America (reviewed in Walker and Cwynar, 2006), Eurasia (reviewed in Brooks, 2006), and more recently the method has been applied in the Southern Hemisphere in Patagonia (Massaferro and Larocque, 2013; Massaferro *et al*., 2014), Central America (Wu *et al*., 2014), East Africa (Eggermont *et al*., 2010), and Australasia (Dimitriadis and Cranston 2001; Woodward and Shulmeister 2006).

Transfer functions make a number of underlying assumptions; particularly the environmental variable to be reconstructed is an ecologically important determinant in the system, and environmental variables other than one being reconstructed have a negligible effect on species assemblages (Juggins, 2013). Rarely are ecological systems as simple as transfer functions would imply and violations of these assumptions will undermine the validity of the environmental reconstruction (Juggins, 2013). Nevertheless, despite known inherent problems associated with transfer functions (Huntley, 2012; Juggins, 2013; Velle *et al*., 2010), quantitative reconstructions from chironomid assemblages often produce consistent results that compare well with other proxy estimates of past temperature (Brooks, 2000; Brooks *et al.*, 2012; Heiri *et al*., 2007). The best performing inference models can reconstruct temperatures with errors of *c.* 1°C (Brooks and Birks, 2001; Eggermont et al., 2010; Heiri et al., 2003; Olander et al., 1999a; Rees et al., 2008; Self et al., 2011) providing high resolution insights into past changes in climate (Brooks and Langdon, 2014), and validation of climate models (Heiri *et al.*, 2014).

1.1 Holocene climate variability

Holocene climate variability is subdued (±2-3^{o}C) (Mayewski *et al*., 2004; O'Brien *et al.*, 1995) compared with the preceding Late Glacial (*c.* 15,000-11,700 years before present [yrs BP], ±7-10^{o}C) (Alley, 2000; Anderson, 1997), nevertheless rapid climate change events are recognised in Holocene palaeoclimate records (Marcott et al., 2013; Mayewski et al., 2004). Changes in insolation caused by solar forcing generally regarded as the dominant driver of global climate change during the Holocene (Mayewski *et al.*, 2004; Wanner *et al*., 2008). The Roman warm period (250 BC-400 AD [2200-1550 yrs BP]), and cooling during the Little Ice Age (LIA) (1350-1850 AD [600-100 yrs BP]) are well established features, notably across the Northern Hemisphere (Johnsen *et al*., 2001; O'Brien *et al*., 1995). Some evidence from the tropics suggests Holocene climate fluctuations such as the LIA maybe global events (Thompson *et al*., 2002; Wanner *et al.*, 2008); however, additional quantitative palaeoclimate records are needed to understand the expression of such events in the tropics, and to clarify global climate teleconnections. Although the low latitudes receive 47% of planetary insolation, the climate response in the tropics to solar variability is poorly understood (Crowley, 2000; Polissar *et al.*, 2006).

1.2 Holocene climate variability in tropical South America

The most notable feature of current South American climate is the annual migration of the Intertropical Convergence Zone (ITCZ), which affects rainfall patterns across the tropical Andes (Garreaud et al., 2009; Hastenrath, 2012). On Holocene timescales, however, there remain large uncertainties regarding the patterns and processes of climate change in the Andes with evidence for both rapid (*c.* 100-1000 yr) precipitation (Haug *et al*., 2001) and temperature (Thompson *et al*., 2006; Wanner *et al.*, 2008). A further point to note is the spatial heterogeneity of Holocene climate variability in the tropical Andes (Baker and Fritz, 2015a), particularly regarding precipitation. Ice core records from the Peruvian and Bolivian Andes since *c*. 5400 cal yrs BP suggest the overall trend is towards a drier climate with high amplitude fluctuations and periods of significant aridity. Precipitation reached a minimum during the period between 3800-2800 cal yrs BP and the LIA (Haug *et al*., 2001; Thompson *et al*., 1986; Thompson *et al*., 1995). Speleothem records from the Central Andes of Peru contradict this, however, and indicate instead that from the 15th to 18th century precipitation was on average about 10% higher than the present day (Reuter *et al*., 2009).

The mid- to late-Holocene (*c.* 6000 cal yrs BP to present) is a period of cooling climate in South America. Pollen evidence suggests montane vegetation replaced Andean forest taxa as the treeline lowered with modern vegetation patterns becoming established by *c.* 3000 cal yrs BP (Markgraf, 1989). Long-term cooling in the late Holocene culminated in a minimum during the 17th and 18th centuries, coinciding with evidence for precipitation minimum during the LIA in northern South America (Haug *et al*., 2001; Thompson *et al*., 1986; Thompson *et al*., 1995). Further south, Patagonian proxy records infer periods that were wet and cold enough to allow glacial advance (Meyer and Wagner, 2008). In the South American tropics, where the relationship between changes in temperature and precipitation are complex (Baker *et al*., 2001; Garreaud *et al*., 2009), more independent quantitative estimates of past temperature are needed in order to resolve climate patterns over the tropical Andes during the Holocene.

1.3 Aims

In this study, we have developed the first chironomid-based temperature calibration data set from the tropical Andes (0 to 17°S). Surface sediment samples from 59 lakes along the eastern flank of the Andes to

105 Amazonia are analysed. Two approaches are used to develop the inference model, the widely used weighted
106 averaging method (Brooks and Birks, 2000) and a Bayesian approach (Holden *et al*., 2008) which has rarely been
107 used before. The models are applied to fossil chironomid assemblages in a late-Holocene lake sediment record
108 from Laguna Pindo, central Ecuador, to reconstruct mean annual temperature (MAT) changes over the past *c.*
109 3000 years.

110

111 **2 Study Sites**

112 **2.1 Modern calibration dataset**

113 Surface sediments were collected from 59 lakes across Bolivia (15 lakes), Peru (32 lakes) and Ecuador (12
114 lakes) between 2004 and 2013 over an altitudinal gradient from 150 m above sea level (a.s.l) to 4655 m a.s.l,
115 between 0-17°S and 64-78°W (Fig 1). The study sites cover an MAT of 25°C; the coldest lake in the data set is
116 0.8°C MAT and the warmest is 25°C MAT (Table 1). The deepest lake is 25 m and the shallowest is 0.1 m, mean
117 water depth of all the study sites is 5 m. Cold, high elevation lakes are more common within the calibration data
118 set and there are no lakes between 16°C and 20°C. Sediment samples used in this study were taken from the
119 uppermost centimetre (0-1cm) which represents the most recent deposits (approx. 5-20 years) (Frey, 1988) and
120 therefore most comparable with the available climate data for calibration.

121

122 **2.2 Fossil chironomid record**

123 Laguna Pindo is a small shallow lake on the eastern flank of the Ecuadorian Andes (1°27.132'S;
124 78°04.847'W) (Fig1). The site is located at an elevation of 1248 m a.s.l. MAT is *c.* 20°C with little seasonal
125 variation and mean annual precipitation (MAP) can reach *c.* 4000 mm per year (Hijmans *et al*., 2005). Currently
126 the lake is not directly fed by a stream in-flow and has no visible stream out-flow; the lake receives water from
127 surface run-off and direct precipitation. There are no obvious geomorphological causes for the escarpment of
128 the lake and we hypothesise it is tectonic in origin.

129 At the time of field work (January 2013) maximum water depth was *c.* 1 m, the lake is heavily overgrown
130 with aquatic macrophytes making a detailed bathometric survey difficult. A sedimentary sequence 929 cm long

was extracted using a cam-modified piston Livingston corer (Colinvaux *et al*., 1999) from the centre of the lake to minimise the chance of encountering a sedimentary gap caused by any periods of lake area reductions. Sediments were recovered in aluminium tubes and sealed on site before being transported to the UK and stored at *c.* 4°C. A total of 6 samples were analysed for ^{14}C radiocarbon using AMS dating at the SUERC radiocarbon facility, East Kilbride (Table 2). An age-depth model was created using version 2.2 of the statistical package clam.R (Blaauw, 2010) and the Southern Hemisphere calibration curve SHCal13.14C (Hogg *et al.*, 2013) (Fig 2). The sampling interval for chironomid analysis was not uniform due to a varied sedimentation rate. To achieve as even a coverage possible over the time interval, samples were taken between every 10 and 20cm.

3. Methods

3.1 Chironomid analysis

Chironomid preparation and identification from both lake surface and core sediments followed standard methods as described by Brooks *et al* (2007). The wet sediment was deflocculated in 10% KOH for 2 minutes at 75°C. The sediment was then washed through 212µm and 90µm sieves with water. Chironomids were picked from the residues in a Bogorov counting tray using a stereomicroscope at 25x magnification. Head capsules were mounted in Euparal, ventral side up and identified to the highest possible taxonomic resolution under a compound light microscope at 200-400x magnifications with reference to Wiederholm (1983), Epler (2001) Rieradevall & Brooks (2001), Brooks *et al* (2007), Cranston (2010) and local taxonomic works including Prat *et al* (2011), and Trivinho-Strixino (2011). Some taxa could not be formally identified and so were given informal names. Images and descriptions of informally named taxa are provided in Matthews-Bird *et al* (2015).

3.2 Environmental variables

Environmental variables (depth, pH, conductivity, and water temperature) were measured at each lake in the field. Organic content of the sediment was established through Loss-on-ignition following standard methods as described by Heiri et al (2001). Climate data (MAT, MAP) were obtained from high resolution, interpolated climate surfaces (Hijmans *et al*., 2005). A summary of all the environmental variables measured can be found in Table 1.

158

159 **3.3 Exploratory statistics**

160 Detrended Correspondence Analysis (DCA) was initially used as an indirect ordination method to assess the
161 gradient lengths in compositional units of taxon turnover (Hill and Gauch, 1980). The gradient length of DCA axis
162 1 was 5.2 standard deviation units (SD), which suggests a unimodal response, and that linear ordination
163 methods were not appropriate (ter Braak, 1987). Canonical Correspondence Analysis (CCA) was used to explore
164 the influence of the measured environmental variables on the distribution and abundance of taxa. Highly
165 correlated variables were partialled-out by analysis of the variance of their regression coefficients indicated by
166 their Variance Inflator Factors (VIFs). Variables with high VIFs were systematically removed from the
167 environmental variable data set until the remaining variables had VIFs below 20. Detrended canonical
168 correspondence analysis (DCCA) was used to test how much of the variance in the assemblage data was
169 explained by each individual explanatory variable. The ratio of λ_1:λ_2 (i.e., the ratio of first constrained DCCA axis
170 1 and second unconstrained DCA axis 2) was used to assess the influence an explanatory variable has in
171 describing the variance in the chironomid community assemblage, and hence its predictive power (Juggins,
172 2013). All taxa were retained in the statistical analysis and rare taxa were down-weighted in the weighted
173 average transfer function (down-weighting of rare species is implicit in the Bayesian approach). Multivariate
174 analysis was carried out on square root transformed chironomid percentage data.

175 Inference models were developed using two separate approaches. The first method relied on weighted
176 averaging methods, a tried and tested technique well established in quantitative palaeoecology (Birks, 1998;
177 Birks *et al*., 2012; ter Braak and Juggins, 1993; ter Braak and Looman, 1986). The second method uses a
178 Bayesian approach, which in general has received less attention (Holden *et al.*, 2008). There are a number of
179 inherent problems associated with quantitative inference models (Huntley, 2012; Juggins, 2013; Velle et al.,
180 2010) so the two independent methods were used to compare results and assess the strengths and weaknesses
181 of each method.

182 The assemblage data was unimodal suggesting transfer functions using weighted averaging partial least
183 squares (WA-PLS) were appropriate (ter Braak and Juggins, 1993). Inference models were also developed using
184 classical and inverse weighted averaging (WA) to compare performance. The optimal number of components

was assessed using leave-one-out cross validation (jack knifing) and a minimum 5% change in prediction error between components. Sample specific errors for the inferred temperatures were obtained through bootstrapping 999 cycles.

Bayesian model selection was used to generate probability-weighted species response curves (SRCs) for each taxon in the calibration dataset. Each taxon is assigned 8,000 possible SRCs. Each of these SRCs has a probability weight based on its relative ability to describe the training data for that taxon. To perform a reconstruction, likelihood functions (temperature probability distributions) are derived from each taxon in a fossil sample, considering all 8,000 SRCs. Combining the likelihood functions of all the taxa in the fossil sample derives the reconstruction. The power of the Bayesian approach is that it ascribes a probability distribution to the reconstruction, providing a reconstruction-specific uncertainty. An important benefit is that all taxa in the sample provide potentially useful information, even those with low counts that would be largely neglected in a weighted averaging approach. To illustrate, a few counts of a taxon with a narrow temperature tolerance may constrain the Bayesian reconstruction more than a very high count of a taxon with a broad tolerance.

Although the Bayesian model was developed for application to pH reconstructions from diatom assemblages, it is generally applicable whenever it is appropriate to assume a unimodal species response to an environmental gradient. The only modification required is the specification of appropriate priors. The *a priori* probability distribution for optimum temperature in the SRCs was assigned to be uniform in the range -4.2 to +30.8°C (training set range ±°5C). The *a priori* probability for SRC tolerance was assigned to be uniform in the range 2 to 10°C. Other SRC priors were unchanged from those in Holden *et al*. (2008).

DCCA detrending by segments, non-linear rescaling, and constrained by radiocarbon age was used to determine compositional turnover constrained within the stratigraphic sequence (Birks and Birks, 2008). The goodness-of-fit to temperature was evaluated by including the fossil chironomid samples passively in a CCA ordination space of the modern training set samples constrained by MAT. Fossil samples with a squared residual distance within the extreme 10% of the modern calibration dataset samples are considered as having a poor fit to temperature. The modern analogue technique was used to test if fossil samples had good analogues within the modern calibration data set. Any fossil sample with a squared chord distance larger than the 95% threshold of the calibration data set is considered to have no good modern analogues (Birks, 1998; Velle *et al*., 2005).

Data were untransformed prior to analysing the dissimilarity using the modern analogue technique. The significance of the final reconstruction was tested by comparing the amount of variance in the fossil data explained by that reconstruction, compared with inferences produced by transfer functions trained on randomly generated environmental data (Telford and Birks, 2011a). In this case, 999 random environmental variables were generated in order to produce the null distribution.

4. Results

4.1 Calibration data set

The eight remaining explanatory variables, after those with VIFs >20 were removed; together explain 34.03% of the variance (Fig 3). The first two CCA axes explained 61.7% of the variance (λ_1=0.792, λ_2 = 0.466). MAT describes most of the variance in the chironomid assemblages and has the highest λ_1:λ_2 ratio (Table 3). When used as a single explanatory variable, MAT explains 12.93% of the variance (λ_1/λ_2= 1.431).

In total, 55 chironomid taxa were identified in the 59 training set lakes. *Chironomus anthracinus*-type was the most widespread taxon, occurring over the entire temperature gradient (Fig 4). Orthocladiinae are generally most abundant towards the cold end of the temperature gradient. *Cricotopus/Paratrichocladius* type III is the dominant taxon of the coldest lake and is not present in sites >10°C MAT. Figure 4 shows the weighted average and Bayesian optima and tolerance of each taxon ordered by lowest to highest optima as modelled in the weighted averaging approach. In general the temperature optima predicted by each method are similar, however, *Tanytarsus* type II and *Cricotopus/Paratrichocladius* type VII have colder optima when modelled using a Bayesian approach. *Cricotopus/Paratrichocladius* type IV has the coldest temperature optimum *c.* 3.3°C (Fig 5). Few Chironominae were found at the cold end of the calibration data set, but, for example, *Parachironomus* and *Tanytarsus* type II were only found in lakes cooler than *c.* 8°C and had optima of *c*. 7.5°C and *c*. 6.5°C respectively. *Paratanytarsus* and *Pseudosmittia* are important components of the chironomid assemblage between 4-12°C, forming >50% of the chironomid community in some lakes, and have optima of *c*. 9.1 and 8.3°C respectively. *Tanytarsus* type I, *Micropsectra* and *Einfeldia* are dominant taxa at mid-temperatures between *c*. 10-22°C. The absence of lakes between *c*. 16°C and *c*. 20°C limits a complete understanding of the distribution of taxa occurring at these temperatures.

DCCA analysis, constrained by MAT, indicates an assemblage shift across the temperature gradient of 2.2 SD units. The biggest change in assemblage composition occurs above 12°C MAT (Fig 4). *Goeldichironomus*, *Cladotanytarsus* and *Tanytarsus* type III were only found in lakes with MAT warmer than *c.* 22°C. Tanypodinae were in greatest abundance at the warm end of the temperature gradient between *c.* 10-26°C, *Procladius* was the most common Tanypodinae. It occurred between *c.* 10-26°C and had an optimum of *c.* 21°C. Both methods (WA and Bayesian) produced similar performance statistics. The best performing model using conventional statistical methods was a WA (inverse) model (Table 4, Fig 6)(R^2_{jack}= 0.890, $RMSEP_{jack}$ = 2.404(°C), Mean $bias_{jack}$= -0.017(°C), Max $bias_{jack}$=4.665(°C)). The Bayesian method produced a slightly higher performing model with R^2_{jack}= 0.909, $RMSEP_{jack}$ =2.373(°C), Mean $bias_{jack}$= 0.598(°C), Max $bias_{jack}$= 3.158(°C).

4.2 Laguna Pindo fossil chironomids and dating

Chironomid remains were found only in the upper 416 cm of the 929cm sequence of Laguna Pindo (Fig 7). In total, 2489 individual chironomid head capsules were analysed. The entire assemblage was made up of 32 taxa in 26 genera and 4 subfamilies. Among the taxa identified, 17 were Chironomini, eight Orthocladiinae and three Tanypodinae. There was high variation between samples both in number of head capsules (average: 82; range: 24 - 184) and concentration per gram of wet sediment (average: 73; range: 2 - 163). There was a marked decline in head capsule concentration below 200 cm. In younger sediments (200-0 cm) head capsule concentration averaged 106/gram, in older samples (200-420 cm) the average was 44/gram. Five zones were identified using optimal partitioning with a broken stick model to define significant zones. *Polypedilum nubifer*-type, *Procladius* and *Limnophyes* were the most abundant taxa; abundances are over 10% wherever they occurred. *Tanytarsus* type II was most abundant below 200 cm (1500 cal yr BP) whilst *Polypedilum nubifer*-type was present in low numbers below 340 cm (2300 cal yr BP). During periods of low *Polypedilum nubifer*-type abundance, *Tanytarsus* type II and *Tanytarsus* type I occur in greater numbers (e.g. 420-360; 290-250 cm).

The best-fit age depth model for Laguna Pindo was a smooth spline (Fig 2). Due to the absence of chironomids at the bottom of the sequence, six radiocarbon samples were used for building the model with a total depth of the sediment considered of 461 cm (Table 2). The sedimentation rate ranged between 0.03 and

0.5 cm/yr, with a sampling interval resolution of 97 years between samples on average (range from 27 to 196 years).

4.3 Palaeotemperature reconstruction

Both transfer functions (WA inverse and Bayesian) show similar patterns in the temperature reconstruction (Fig 8). From 3000-2500 cal yr BP inferred temperatures are cold relative to the modern (20.2°C). The minimum WA inverse temperatures are much colder (13.5°C±2.5) than the inferred Bayesian temperatures (17.5°C±3.7) for the early section of the sequence. From 2400 to 1700 cal yr BP inferred temperatures from both methods oscillate around *c.* 18-19°C but remained depressed relative to the modern. A notable feature of both reconstructions is the sudden drop in inferred temperatures at 1600 cal yr BP. Inferred temperatures fall by *c.* 2°C to 17.5°C±2.7. This abrupt drop in temperature is short-lived in both reconstructions and temperatures return to previous values in the subsequent sample. From 1500 cal yr BP to the present the chironomid-inferred temperatures stabilise and steadily rise. Peak temperatures for the entire record (21.9°C±3.5) are inferred between 400-700 cal yr BP. Temperatures begin to cool from 400 cal yrs BP in both reconstructions, reaching a minimum of *c.* 17°C±2.5 *c.* 100 cal yr BP before rising rapidly to between 20-21°C±2.5 in the most recent sediment sample. On average the Bayesian model infers warmer temperatures than the WA model.

The fossil samples of Laguna Pindo plot within the modern variation of chironomid assemblages when included passively in a CCA analysis of the calibration data set (Fig 9). This suggests that the calibration dataset is appropriate for the fossil sequence of Laguna Pindo. The fossil samples plot along the MAP gradient suggesting precipitation is an important variable controlling the variance in the fossil assemblages. The sites associated with high precipitation in the calibration dataset are located in the same region of the Ecuadorian Andes as the fossil site. With a modern MAT of *c.* 20°C, however, Laguna Pindo is located in a region of the temperature gradient that is poorly covered in the calibration dataset (Fig 4). Seven taxa found in the Laguna Pindo sequence do not occur in any of the analysed calibration data set lakes. These include three unknown morphotypes, three *Xestochironomus* morphotypes, and *Metriocnemus eurynotus*-type. These taxa, however, never comprise more than 10% of the chironomid assemblage of any one sample.

Fourteen of the fossil samples are considered to have a poor goodness-of-fit to temperature and all fossil samples are considered as having poor modern analogues in the calibration data set (Fig 10). Although the

291 modern analogue technique is not used to infer past temperatures the lack of modern analogues in the fossil
292 assemblage is important when considering the reliability of any reconstruction.

293 DCCA constrained by radiocarbon age shows an abrupt change at 1475 cal yr BP between zones 3 and 4
294 and a turnover of 1.6 SD units over the whole sequence (Fig 10). Much of the variation in goodness-of-fit and
295 DCCA sample scores is mirrored by changes in count size and head capsule concentration. The sudden drop in
296 head capsule concentration occurs at a step change in DCCA assemblage variation (1475 cal yrs BP) (Fig 10).
297 Periods of increased count size and head capsule concentration in older sediments (2100-2250 cal yrs BP) also
298 coincides with periods of improved goodness-of-fit (Fig 10). The WA classical inferred MAT values using the
299 modern calibration data set explain more of the variance than 95% of randomly generated variables and so the
300 WA classical MAT reconstructions can be deemed statistically significant (p= 0.032) (Fig 11) (Telford and Birks,
301 2011a).

302

303 **5. Discussion**

304 **5.1 Chironomids and environmental variables**

305 Chironomids have been shown to respond to temperature at a variety of spatial scales and taxonomic levels
306 (Brooks, 2006; Eggermont and Heiri, 2011). Temperature is a key variable in controlling chironomid
307 development at all stages of their life cycles, and influences voltinism, behaviour and metabolism (Armitage *et*
308 *al*., 1995). Across the Northern Hemisphere, over large temperature gradients, mean July air temperature, the
309 warmest month of the year, which reflects the developmental period of most species, has been shown to be the
310 major determinant of variation in chironomid assemblages (Brooks, 2006; Walker and Cwynar, 2006). As a
311 result, many quantitative temperature inference models have been developed to reconstruct mean July air
312 temperature. Across the tropics however seasonal variation is small and many chironomids are multivoltine
313 (Walker and Mathews, 1987) so temperatures throughout the year are likely to be relatively more influential. In
314 tropical East Africa, Eggermont *et al*. (2010) demonstrated that mean annual air temperature was a significant
315 driver of chironomid assemblage composition and developed a chironomid-based inference model on this basis.
316 Similarly, Wu *et al*. (2014) showed MAT to be the most important environmental variable when developing a
317 chironomid inference model for Central America. When attempting to make quantitative inferences from fossil

assemblages it is first crucial to establish that the variable of interest is an important ecological determinant. The variable to be reconstructed must describe a statistically important component of the variance within the assemblage data (Juggins, 2013). Compared to other measured variables, mean annual temperature explained the largest amount of chironomid assemblage variance and had the highest eigenvalue ratio (λ_1:λ_2) in the Andean calibration dataset (Table 3). The explanatory strength of temperature in the calibration data set meets the minimum criterion proposed by Juggins (2013) (i.e. λ_1:$\lambda_2 > 1.0$) for temperature being a suitable variable to reconstruct from this calibration dataset.

The DCCA results suggest that precipitation is also a strong ecological determinant (λ_1:λ_2=0.9); the passive plot of fossil samples with calibration samples further supports this conclusion. The fossil samples of Laguna Pindo are strongly associated with MAP. Precipitation in Andean landscapes, however, is spatially heterogeneous and geographically close localities experience significantly different rainfall patterns (Garreaud *et al*., 2009). Lakes associated with high rainfall (Fig 3) are actually in areas of the northern Andes with two rainy seasons a year. It is very likely that the bimodality of rainfall in these areas is as important in controlling chironomid populations as the total amount of rainfall as measured by MAP. Precipitation is also intrinsically linked to temperature as both temperature and precipitation increase with decreasing latitude in tropical South America (Garreaud *et al*., 2009). Unlike temperature, precipitation affects chironomids indirectly making any quantitative inference difficult. Precipitation will alter a suite of environmental variables (e.g. pH, conductivity, depth, substrate) making quantitative inferences of precipitation problematic. As chironomid life cycles are strongly controlled by temperature and many tropical chironomid species tend to be multivoltine, we suggest the most appropriate variable both ecologically and statistically to reconstruct using the Andean calibration data sets is MAT although the of influence of precipitation cannot be overlooked.

The optima and temperature tolerances (Fig 5) of many taxa found in the current study are similar to that noted in other Neotropical chironomid calibration datasets, further supporting the conclusion of temperature being an important ecological determinant. For example, Wu *et al*. (2014) in Central America, found taxa of the genera *Beardius*, *Labrundinia* and *Goeldichironomus* to have optima between 23-24°C whilst *Limnophyes* and *Corynoneura* where more abundant at the colder end of the gradient with optima of 15°C and 18°C respectively. In the current dataset *Beardius, Labrundinia*, and *Goeldichironomus* all have optima between

23-24°C and *Limnophyes* and taxa of *Corynoneura* also have optima of 15°C and 19°C, respectively. *Limnophyes* also has one of the broadest tolerances of all taxa in both calibration datasets suggesting the genus is probably represented by many species (Matthews-Bird et al., 2015). More work is needed in order to refine chironomid larval taxonomy in South America, however the current data suggest the potential for a larger calibration dataset applicable to wider area incorporating the Northern Neotropics and Central America.

5.2 Model performance

Although both models (WA inverse and Bayesian) perform well (WA RMSEP= 2.4°C/ 9.6% of training set range and Bayesian RMSEP= 2.3°C/9.2% of training set range), some of the best performing chironomid-based temperature inference models have prediction errors closer to 1.0°C (Brooks and Birks, 2001; Heiri *et al*., 2011, 2007; Olander *et al*., 1999). The highest performing chironomid inference models often have in excess of 100-150 calibration sites compared with just 59 in the current model and this may account for its reduced performance. Furthermore the lakes in the calibration data set are not evenly distributed over the temperature gradient. The cold end of the gradient has a higher number of lakes (34 cold, high elevation lakes) than at warm and intermediate temperatures (15 warm, mid-low elevation lakes). Uneven sampling has been shown to lead to biases which may reduce RMSEP (Telford and Birks, 2011b). Furthermore the over-representation of cold lakes in the current dataset may result in under-estimation of the temperature optima of some taxa and, therefore, bias temperature estimates towards cold values. In the Andean dataset, as analysis of residuals shows, temperatures around 10°C are often under-estimated (Fig 6). Furthermore, the inferred temperatures of Laguna Pindo are on average cooler than the modern day conditions.

The absence of lakes in part of the temperature gradient may limit the reliability of estimates of optima and tolerances of taxa and also create 'edge effects' in the middle of the temperature range, in addition to those that occur at the cold and warm end of the temperature gradient (Eggermont *et al*., 2010). Such problems are inherent to WA models as predicted values are pulled towards the mean of the training set resulting in under- and over-estimations of high and low values (ter Braak and Juggins 1993). However, despite having no lakes between 16-20°C in the calibration data set, additional edge effects are not a feature of the current

inference model. The gap of c. 4°C does not appear to have compromised model performance, probably as the interval is not significant and taxa have tolerances that span these temperatures.

Chironomid larval head capsule concentrations can vary significantly between lakes, due to differences in preservation or abundance. Low counts can have adverse effects on the performance of inference models and the reliability of quantitative environmental reconstructions when using conventional methods (Heiri and Lotter, 2001; Quinlan and Smol, 2001). A minimum count size of 50 head capsules per sample is advised (Heiri and Lotter, 2001; Quinlan and Smol, 2001), however, good model performance has been achieved even when several samples include as few as 15-30 head capsules (Massaferro *et al*., 2014). In some lakes in the current training set head capsule concentrations were as low as two head capsules per gram of sediment. Fifteen lakes in the data set produced fewer than 50 head capsules, and three lakes had fewer than 30. On average 77 individuals were analysed from each lake with a minimum count of 23 and a maximum of 164 (Table 1). Lakes with low head capsule counts were retained in the model in order to maintain as even coverage as possible across the temperature gradient.

Polypedilum nubifer-type and *Chironomus anthracinus*-type make up a large component of the chironomid assemblages in lakes across the entire temperature gradient (Fig 4). Such eurythermic taxa probably include several different species. It is difficult to model reliable, or even meaningful, optima for eurythermic taxa. Poor model performance or unreliable reconstructions may result if the assemblage is dominated by eurythermic taxa. We note that eurythermic taxa are described by high tolerance SRCs in the Bayesian approach, leading to increased uncertainty in reconstructions through broad likelihood functions that contribute little information to the posterior. Inferred temperature of *c.* 10°C, are likely to be underestimated as many taxa found at these temperatures also occur in cold lakes, which are over-represented in the calibration data-set. In African lakes Eggermont *et al*. (2010) found that the presence of eurythermic taxa such as *Chironomus* type Kibos caused an overestimation of temperatures in lakes at the warm end of the gradient. They also found that the occurrence of *Limnophyes minimus*-type and *Paraphaenocladius* type OI Bolossat overestimated the temperature of lakes close to where gaps occurred in the gradient (Eggermont *et al*., 2010). Similarly, in a New Zealand calibration data set developed by Woodward and Shulmeister (2006), *Chironomus*

was present in both high elevation, cold, oligotrophic lakes and lower elevation, warm, eutrophic lakes. The intermediate temperature optimum estimated for this taxon resulted in over-estimated temperatures of cold lakes and under-estimates of warm lakes (Woodward and Shulmeister, 2006). Eurythermic taxa may be contributing to the over-estimation of cold temperatures and the under-estimation of temperatures in the middle of the gradient in the Andean inference model.

5.3 WA vs Bayesian

Despite similar performance statistics between the Bayesian and WA methods, the inferred pattern of late-Holocene temperature change is different. Temperatures inferred c. 2700 cal yr BP (400 cm) (Fig 8) using the WA inverse method is extremely cold (*c.* 14°C) compared with the rest of the record. This reconstruction is driven by the high abundance of *Tanytarsus* type II, a taxon that has a WA temperature optimum of 6.5°C. The Bayesian reconstruction for this sample of 17.8 ±2.8°C, is in line with more modest temperature shifts that would be expected in the late-Holocene (Wanner *et al*., 2008). One advantage of the Bayesian methodology is the transparency of the reconstruction through consideration of individual likelihood functions for this assemblage (Fig 12). Although *Tanytarsus* type II is abundant in the sample its influence in the reconstruction is moderated by several other taxa with higher temperature optima that are present at low abundances. This temperature estimate demonstrates the Bayesian reconstruction can be sensitive to a few counts of a species that have a negligible effect in a WA approach. The likelihood function for Chironomini type II, which has an abundance of only 2.3% in the sample, constrains the reconstruction more than *Tanytarsus* type II, which has an abundance of 74%. This is because Chironomini type II is only found in the warmest lakes in the calibration set, each time with a low abundance. We note that because it is found in only three training set sites, Chironomini type II is associated with many (671) high-probability SRCs, defined as having a probability great that 10% of the most likely SRC. For this reason, its likelihood function is relatively broad and extends to temperatures far lower than the temperature of the sites in which the taxon is found in the training set.

5.4 Temperature and secondary environmental variables

Whilst the λ1/λ2 of 1.431 indicates that MAT is appropriate for reconstruction using this calibration dataset (Juggins, 2013), it does not necessarily mean that reliable temperature reconstructions can be obtained from a fossil record (Telford and Birks, 2011a). Before attempting to interpret any reconstruction several metrics can be used to assess the validity of a reconstruction (Juggins and Telford, 2012).

The modern analogue technique compares the similarity of the fossil samples to the modern samples in the calibration data set. All fossil samples are greater than the 5th percentile of the square chord distance (Fig 10), which suggests there is no close modern analogue in the calibration set to any fossil sample (Birks, 1998; Juggins and Birks, 2001). The lack of modern analogues in the Laguna Pindo fossil sequence is due to the many taxa present in the fossil samples that are not present in the calibration data set. This may reflect the lack of lakes in the calibration dataset with MAT values close to those of Laguna Pindo. Nevertheless, WA and WAPLS models have been shown to perform well in non-analogue situations (Birks *et al*., 2010). The Bayesian method generates temperature reconstructions from likelihood functions of species in the calibration data set. Although analogous assemblages are not required for the Bayesian reconstruction (each taxon is treated equally and individually), species that are absent from the training set cannot contribute information to the posterior, thereby increasing the uncertainty associated with the reconstruction. One advantage of the Bayesian methodology is that this uncertainty is explicitly incorporated into the Bayesian reconstruction (Holden *et al*., 2008).

During periods of poor fit-to-temperature, variables other than temperature may have been affecting the composition of the chironomid assemblage. As noted previously, the CCA biplot of fossil samples included passively with the significant explanatory variables (Fig 9) shows that MAP was also important in driving the assemblage variance. During times of poor fit to temperature the influence of precipitation as a secondary variable may be more important than temperature in influencing the chironomid assemblage composition. Indeed, precipitation has been shown to be an important variable in controlling the modern distribution of chironomid taxa in the tropical Andes (Matthews-Bird et al., 2015).

Samples with poor fit-to-temperature also corresponded with samples having low numbers of head capsules. The number of head capsules retrieved will directly affect how representative a sample is to the chironomid fauna (Heiri, 2004; Quinlan and Smol, 2001). The cold oscillations inferred from the Bayesian

reconstruction are more in line with what is expected during the late-Holocene (1-3°C); the likelihood functions of rare species, which favour warm conditions, combine to rule out the anomalously cold temperatures suggested by some of the WA reconstructions. As discussed above, the over-representation of cold lakes in the calibration dataset will likely bias species optima to colder values in a weighted average approach so there may be a tendency for the model to underestimate temperature, especially during cold periods. This problem is likely exaggerated when head capsule concentration is low, cold indicator taxa may have higher abundances than would be the case if all taxa were accurately represented.

The DCCA results indicate that there was a distinct change in the composition of the chironomid assemblage after 1600 cal yr BP (210 cm). This largely coincides with an increase in head capsule concentration, possibly indicating an increase in lake productivity, and the shift in chironomid-inferred temperatures from low to high. Indeed post 1600 cal yr BP, (210 cm) samples are inferred as being on average 2-3°C warmer than early sections using Bayesian and WA models respectively.

Although the temperature reconstruction has a good ecological basis, because chironomids globally are highly sensitive to temperature and, Laguna Pindo is on an ecotonal boundary that is sensitive to temperature changes, precipitation is influential as a secondary variable. The WA inverse MAT reconstruction, however, is statistically significant based on the criteria described by Telford and Birks (2011a) (Fig 11) suggesting that despite precipitation as a possible confounding variable, a temperature signal can be obtained from Neotropical chironomids. We would caution, however, against an over interpretation at this stage. Due to some of the limitations discussed previously, the reconstruction can only currently be deemed qualitative and requires more research before quantitative estimates can be generated with confidence.

6. Conclusions

The chironomid fauna of the tropical Andes have been shown to be sensitive to climate variables, particularly temperature and precipitation. Both variables (MAT and MAP) meet the basic criteria for being used in an environmental reconstruction using the Andean calibration dataset. MAT, however, is an important determinant of chironomid species distribution and abundance and was therefore more appropriate to be

reconstructed. The influence of precipitation should be explored further and must be considered as an important secondary variable especially when reconstructing past conditions in the region. It is very likely that the influence of precipitation noted here relates to the annual variability in rainfall across the Andes as opposed to overall amount making any quantitative interpretations even more difficult.

The two techniques used to develop inference models (WA and Bayesian) show comparable performance statistics (WA inverse model R^2_{jack}= 0.890, $RMSEP_{jack}$ = 2.404(°C), Mean $bias_{jack}$= -0.017(°C), Max bias $_{jack}$=4.665(°C); Bayesian model R^2_{jack}= 0.909, $RMSEP_{jack}$ =2.373(°C), Mean $bias_{jack}$= 0.598(°C), Max bias $_{jack}$= 3.158(°C)). This work demonstrates a proof of method, however, a larger calibration dataset with a more even coverage of calibration sites is needed in order to improve model performance. The Bayesian approach provided a transparent reconstruction less susceptible to the effect of an uneven distribution of calibration sites and performed particularly well during periods of low count size and when inferring cold intervals. The chironomid-based MAT reconstruction from the Laguna Pindo is often colder than would be expected for Holocene timescales. The underestimated temperatures are most likely the direct result of an over representation of cold lakes in the calibration dataset. The addition of more calibration sites between 12°C and 20°C would expand our understanding of tropical Andean chironomid distribution, and significantly improve model performance and reconstruction reliability.

Knowledge of past tropical climate dynamics is fundamental not only to understanding regional climate but also global climate patterns and hemispherical teleconnections. Quantitative temperature proxies, such as chironomids, will provide valuable data on past climate variability in the region. The reconstructions presented here demonstrate the potential of the proxy and also highlights the complexity of late-Holocene climate change in tropical South America.

Acknowledgements

Funding was provided by the Natural Environment Research Council (NERC), UK. NERC grant (ref: NE/J018562/1) was awarded to E. Montoya and (ref: NE/J500288/1) awarded to F. Matthews-Bird. This work was supported by the NERC Radiocarbon Facility NRCF010001 (allocation number 1682.1112). Special thanks to

Dr Pauline Gulliver for her continuous involvement and support during radiocarbon dating. The authors also wish to thank Mark Bush, Francis Mayle, Yarrow Axford, Alex Chepstow-Lusty and Mick Frogley for their kind donation of samples. Data is stored with the National Geoscience Data Centre (NGDC) and can be found at http://www.bgs.ac.uk/downloads/home.html.

References

Alley, R.B., 2000. The Younger Dryas cold interval as viewed from central Greenland. Quat. Sci. Rev. 19, 213–226.

Anderson, E.D., 1997. Younger Dryas research and its implications for understanding abrupt climatic change. Prog. Phys. Geogr. 21, 230–249.

Armitage, P.D., Cranston, P.S., Pinder, L.C.V., 1995. The Chironomidae: the biology and ecology of nonbiting midges. London: Chapman and Hall.

Baker, P. a., Fritz, S.C., 2015b. Nature and causes of Quaternary climate variation of tropical South America. Quat. Sci. Rev. 124, 31–47. doi:10.1016/j.quascirev.2015.06.011

Baker, P.A., Seltzer, G.O., Fritz, S.C., Dunbar, R.B., Grove, M.J., Tapia, P.M., Cross, S.L., Rowe, H.D., Broda, J.P., 2001. The history of South American tropical precipitation for the past 25,000 years. Science 291, 640–643. doi:10.1126/science.291.5504.640

Bird, B.W., Abbott, M.B., Vuille, M., Rodbell, D.T., Stansell, N.D., Rosenmeier, M.F., 2011. A 2,300-year-long annually resolved record of the South American summer monsoon from the Peruvian Andes. Proc. Natl. Acad. Sci. U. S. A. 108, 8583–8. doi:10.1073/pnas.1003719108

Birks, H.J.B., 1998. Numerical tools in palaeolimnology–Progress, potentialities and problems. J. Paleolimnol. 20, 307–332.

Birks, H.J.B., Birks, H.H., 2008. Biological responses to rapid climate change at the Younger Dryas-Holocene transition at Krakenes, western Norway. The Holocene 18, 19–30. doi:10.1177/0959683607085572

Birks, H.J.B., Heiri, O., Seppä, H., Bjune, A.E., 2010. Strengths and Weaknesses of Quantitative Climate Reconstructions Based on Late-Quaternary Biological Proxies. Open Ecol. J. 3, 68–110.

Birks, H.J.B., Lotter, A.F., Juggins, S., Smol, J.P. (Eds.), 2012. Tracking Environmental Change Using Lake Sediments; Data Handling and Numerical Techniques. Springer Netherlands.

Blaauw, M., 2010. Methods and code for "classical" age-modelling of radiocarbon sequences. Quat. Geochronol. 5, 512–518. doi:10.1016/j.quageo.2010.01.002

Brooks, S.J., 2006. Fossil midges (Diptera: Chironomidae) as palaeoclimatic indicators for the Eurasian region. Quat. Sci. Rev. 25, 1894–1910. doi:10.1016/j.quascirev.2005.03.021

Brooks, S.J., 2000. Chironomid-inferred Late-glacial air temperatures at Whitrig Bog, Southeast Scotland. J. Quat. Sci. 15, 759–764.

Brooks, S.J., Axford, Y., Heiri, O., Langdon, P.G., Larocque-Tobler, I., 2012. Chironomids can be reliable proxies for Holocene temperatures. A comment on Velle et al. (2010). The Holocene 22, 1495–1500. doi:10.1177/0959683612449757

Brooks, S.J., Birks, H.J.B., 2001. Chironomid-inferred air temperatures from Lateglacial and Holocene sites in

north-west Europe: progress and problems. Quat. Sci. Rev. 20, 1723–1741. doi:10.1016/S0277-3791(01)00038-5

Brooks, S.J., Birks, H.J.B., 2000. Chironomid-inferred late-glacial and early-Holocene mean July air temperatures for Kråkenes Lake, western Norway. J. Paleolimnol. 23, 77–89.

Brooks, S.J., Langdon, P.G., 2014. Summer temperature gradients in northwest Europe during the Lateglacial to early Holocene transition (15–8 ka BP) inferred from chironomid assemblages. Quat. Int. 1–11. doi:10.1016/j.quaint.2014.01.034

Brooks, S.J., Langdon, P.G., Heiri, O., 2007. The Identification and use of Palaearctic Chironomidae Larvae in Palaeoecology. QRA Technical Guide No. 10, Quaternary Research Association, London.

Čiamporová-Zaťovičová, Z., Hamerlík, L., Šporka, F., Bitušík, P., 2010. Littoral benthic macroinvertebrates of alpine lakes (Tatra Mts) along an altitudinal gradient: a basis for climate change assessment. Hydrobiologia 648, 19–34. doi:10.1007/s10750-010-0139-5

Colinvaux, P., De Oliveira, P.E., Patino, J.E.., 1999. Amazon Pollen Manual and Atlas. Harwood Academic Publishers.

Collins, M., An, S.-I., Cai, W., Ganachaud, A., Guilyardi, E., Jin, F.-F., Jochum, M., Lengaigne, M., Power, S., Timmermann, A., Vecchi, G., Wittenberg, A., 2010. The impact of global warming on the tropical Pacific Ocean and El Niño. Nat. Geosci. 3, 391–397. doi:10.1038/ngeo868

Cranston, P.S., 2010. URL http://chirokey.skullisland.info/.

Crowley, T.J., 2000. Causes of Climate Change Over the Past 1000 Years. Science. 289, 270–277. doi:10.1126/science.289.5477.270

Dimitriadis, S., Cranston, P.S., 2001. An Australian Holocene climate reconstruction using Chironomidae from a tropical volcanic maar lake. Palaeogeogr. Palaeoclimatol. Palaeoecol. 176, 109–131.

Eggermont, H., Heiri, O., 2011. The chironomid-temperature relationship: expression in nature and palaeoenvironmental implications. Biol. Rev. Camb. Philos. Soc. 87, 430–456. doi:10.1111/j.1469-185X.2011.00206.x

Eggermont, H., Heiri, O., Russell, J., Vuille, M., Audenaert, L., Verschuren, D., 2010. Paleotemperature reconstruction in tropical Africa using fossil Chironomidae (Insecta: Diptera). J. Paleolimnol. 43, 413–435. doi:10.1007/s10933-009-9339-2

Epler, J.H., 2001. Identification manual for the Larval Chironomidae (Diptera) of South Carolina.

Frey, D.G., 1988. Littoral and offshore communities of diatoms, cladocerans and dipterous larvae, and their interpretation in paleolimnology. J. Paleolimnol. 1, 179–191.

Garreaud, R.D., Vuille, M., Compagnucci, R., Marengo, J., 2009. Present-day South American climate. Palaeogeogr. Palaeoclimatol. Palaeoecol. 281, 180–195. doi:10.1016/j.palaeo.2007.10.032

Hastenrath, S., 2012. Climate dynamics of the tropics. Springer Science & Business Media.

Haug, G.H., Hughen, K.A., Sigman, D.M., Peterson, L.C., Röhl, U., 2001. Southward migration of the intertropical convergence zone through the Holocene. Science 293, 1304–8. doi:10.1126/science.1059725

Heiri, O., 2004. Within-lake variability of subfossil chironomid assemblages in shallow Norwegian lakes. J. Paleolimnol. 32, 67–84. doi:10.1023/B:JOPL.0000025289.30038.e9

Heiri, O., Brooks, S.J., Birks, H.J.B., Lotter, A.F., 2011. A 274-lake calibration data-set and inference model for chironomid-based summer air temperature reconstruction in Europe. Quat. Sci. Rev. 30, 3445–3456. doi:10.1016/j.quascirev.2011.09.006

Heiri, O., Brooks, S.J., Renssen, H., Bedford, A., Hazekamp, M., Ilyashuk, B., Jeffers, E.S., Lang, B., Kirilova, E., Kuiper, S., Millet, L., Samartin, S., Toth, M., Verbruggen, F., Watson, J.E., van Asch, N., Lammertsma, E., Amon, L., Birks, H.H., Birks, H.J.B., Mortensen, M.F., Hoek, W.Z., Magyari, E., Muñoz Sobrino, C., Seppä, H., Tinner, W., Tonkov, S., Veski, S., Lotter, A.F., 2014. Validation of climate model-inferred regional temperature change for late-glacial Europe. Nat. Commun. 5, 4914. doi:10.1038/ncomms5914

588 Heiri, O., Cremer, H., Engels, S., Hoek, W.Z., Peeters, W., Lotter, A.F., 2007. Lateglacial summer temperatures in
589 the Northwest European lowlands: a chironomid record from Hijkermeer, the Netherlands. Quat. Sci. Rev.
590 26, 2420–2437. doi:10.1016/j.quascirev.2007.06.017

591 Heiri, O., Lotter, A., 2001. Effect of low count sums on quantitative environmental reconstructions: an example
592 using subfossil chironomids. J. Paleolimnol. 26, 343–350.

593 Heiri, O., Lotter, A.F., Hausmann, S., Kienast, F., 2003. A chironomid-based Holocene summer air temperature
594 reconstruction from the Swiss Alps. The Holocene 13, 477–484.

595 Heiri, O., Lotter, A.F., Lemke, G., 2001. Loss on ignition as a method for estimating organic and carbonate
596 content in sediments: reproducibility and comparability of results. J. Paleolimnol. 25, 101–110.

597 Hijmans, R.J., Cameron, S.E., Parra, J.L., Jones, P.G., Jarvis, A., 2005. Very high resolution interpolated climate
598 surfaces for global land areas. Int. J. Climatol. 25, 1965–1978. doi:10.1002/joc.1276

599 Hill, M., Gauch, H.., 1980. Detrended correspondence analysis: an improved ordination technique. Vegetatio 42,
600 47–58.

601 Hogg, A.G., Hua, Q., Blackwell, P.G., Niu, M., Buck, C.E., Guilderson, T.P., Heaton, T.J., Palmer, J.G., Reimer, P.J.,
602 Reimer, R.W., Turney, C.S.M., Zimmerman, S.R.H., 2013. SHCal13 Southern Hemisphere calibration, 0–
603 50,000 cal yr BP. Radiocarbon 55, 1889–1903.

604 Holden, P.B., Mackay, A.W., Simpson, G.L., 2008. A Bayesian palaeoenvironmental transfer function model for
605 acidified lakes. J. Paleolimnol. 39, 551–566. doi:10.1007/s10933-007-9129-7

606 Huntley, B., 2012. Reconstructing palaeoclimates from biological proxies: Some often overlooked sources of
607 uncertainty. Quat. Sci. Rev. 31, 1–16. doi:10.1016/j.quascirev.2011.11.006

608 Ivanochko, T., Ganeshram, R., Brummer, G., Ganssen, G., Jung, S., Moreton, S., Kroon, D., 2005. Variations in
609 tropical convection as an amplifier of global climate change at the millennial scale. Earth Planet. Sci. Lett.
610 235, 302–314. doi:10.1016/j.epsl.2005.04.002

611 Jansen, E., Overpeck, J., Briffa, K.., Duplessy, J.-C., Joos, F., Masson-Delmotte, V., Olago, D., Otto-Bliesner, B.,
612 Peltier, W.., Rahmstorf, S., Ramesh, R., Raynaud, D., Rind, O., Solomina, O., Villalba, R., Zhang, D., 2007.
613 Climate Change 2007: The Physical Science Basis. Contribution of Working Group I to the Fourth
614 Assessment Report of the Intergovvernmental Panel on Climate Change, in: Solomon, S., Qin, D., Manning,
615 M., Chen, Z., Marquis, M., Averyt, K.B., Tignor, M., Miller, H.. (Eds.), . Cambridge University Press,
616 Cambridge, United Kingdom and New York, NY, USA.

617 Johnsen, S.J., Dahl-Jensen, D., Gundestrup, N., Steffensen, J.P., Clausen, H.B., Miller, H., Masson-Delmotte, V.,
618 Sveinbjornsdottir, A.E., White, J., 2001. Oxygen isotope and palaeotemperature records from six
619 Greenland ice-core stations: Camp Century, Dye-3, GRIP, GISP2, Renland and NorthGRIP. J. Quat. Sci. 16,
620 299–307. doi:10.1002/jqs.622

621 Jomelli, V., Favier, V., Rabatel, A., Brunstein, D., Hoffmann, G., Francou, B., 2009. Fluctuations of glaciers in the
622 tropical Andes over the last millennium and palaeoclimatic implications: A review. Palaeogeogr.
623 Palaeoclimatol. Palaeoecol. 281, 269–282. doi:10.1016/j.palaeo.2008.10.033

624 Jones, P., Mann, M., 2004. Climate over past millennia. Rev. Geophys. 42, 1–42.
625 doi:10.1029/2003RG000143.CONTENTS

626 Juggins, S., 2013. Quantitative reconstructions in palaeolimnology: new paradigm or sick science? Quat. Sci. Rev.
627 64, 20–32. doi:10.1016/j.quascirev.2012.12.014

628 Juggins, S., Birks, H.J.B., 2001. Quantitative Environmental Reconstructions from Biological Data, in: Birks, H.J.B.,
629 Lotter, A.F., Juggins, S., Smol, J.P. (Eds.), Tracking Environmental Change Using Lake Sediments,
630 Developments in Paleoenvironmental Research 5. pp. 431–494.

631 Juggins, S., Telford, R.J., 2012. Exploratory Data Analysis and Data Display, in: Birks, H.J.B., Lotter, A.F., Juggins,
632 S., Smol, J.P. (Eds.), Tracking Environmental Change Using Lake Sediments, Developments in
633 Paleoenvironmental Research 5, Developments in Paleoenvironmental Research. Springer Netherlands,
634 Dordrecht, pp. 123–141. doi:10.1007/978-94-007-2745-8

635 Kanner, L.C., Burns, S.J., Cheng, H., Edwards, R.L., Vuille, M., 2013. High-resolution variability of the South
636 American summer monsoon over the last seven millennia: insights from a speleothem record from the
637 central Peruvian Andes. Quat. Sci. Rev. 75, 1–10. doi:10.1016/j.quascirev.2013.05.008

638 Leng, M.J., Marshall, J.D., 2004. Palaeoclimate interpretation of stable isotope data from lake sediment
639 archives. Quat. Sci. Rev. 23, 811–831. doi:10.1016/j.quascirev.2003.06.012

640 Marcott, S. a, Shakun, J.D., Clark, P.U., Mix, A.C., 2013. A reconstruction of regional and global temperature for
641 the past 11,300 years. Science 339, 1198–1201. doi:10.1126/science.1228026

642 Markgraf, V., 1989. Palaeoclimates in Central and South America since 18,000 BP based on Pollen and lake-level
643 records. Quat. Sci. Rev. 8, 1–24.

644 Massaferro, J., Larocque, I.T., 2013. Using a newly developed chironomid transfer function for reconstructing
645 mean annual air temperature at Lake Potrok Aike , Patagonia , Argentina. Ecol. Indic. 24, 201–210.
646 doi:10.1016/j.ecolind.2012.06.017

647 Massaferro, J., Larocque-Tobler, I., Brooks, S.J., Vandergoes, M., Dieffenbacher-Krall, A., Moreno, P., 2014.
648 Quantifying climate change in Huelmo mire (Chile, Northwestern Patagonia) during the Last Glacial
649 Termination using a newly developed chironomid-based temperature model. Palaeogeogr. Palaeoclimatol.
650 Palaeoecol. 399, 214–224. doi:10.1016/j.palaeo.2014.01.013

651 Matthews-Bird, F., Gosling, W.D., Coe, A.L., Bush, M., Mayle, F.E., Axford, Y., Brooks, S.J., 2015. Environmental
652 controls on the distribution and diversity of lentic Chironomidae (Insecta : Diptera) across an altitudinal
653 gradient in tropical South America. Ecol. Evol. 1–22. doi:10.1002/ece3.1833

654 Mayewski, P.A., Rohling, E.E., Curt Stager, J., Karlén, W., Maasch, K.A., David Meeker, L., Meyerson, E. a., Gasse,
655 F., van Kreveld, S., Holmgren, K., Lee-Thorp, J., Rosqvist, G., Rack, F., Staubwasser, M., Schneider, R.R.,
656 Steig, E.J., 2004. Holocene climate variability. Quat. Res. 62, 243–255. doi:10.1016/j.yqres.2004.07.001

657 Meyer, I., Wagner, S., 2008. The Little Ice Age in southern Patagonia : Comparison between paleoecological
658 reconstructions and downscaled model output of a GCM simulation. PAGES news 16.

659 Mosblech, N. a. S., Bush, M.B., Gosling, W.D., Hodell, D., Thomas, L., van Calsteren, P., Correa-Metrio, A.,
660 Valencia, B.G., Curtis, J., van Woesik, R., 2012. North Atlantic forcing of Amazonian precipitation during the
661 last ice age. Nat. Geosci. 5, 817–820. doi:10.1038/ngeo1588

662 O'Brien, S.R., Mayewski, P. a., Meeker, L.D., Meese, D.A., Twickler, M.S., Whitlow, S.I., 1995. Complexity of
663 Holocene Climate as Reconstructed from a Greenland Ice Core. Science (80-.). 270, 1962–1964.

664 Olander, H., Korhola, a., Blom, T., Birks, H.J.B., 1999a. An expanded calibration model for inferring lakewater
665 and air temperatures from fossil chironomid assemblages in northern Fennoscandia. The Holocene 9, 279–
666 294. doi:10.1191/095968399677918040

667 Olander, H., Korhola, a., Blom, T., Birks, H.J.B., 1999b. An expanded calibration model for inferring lakewater
668 and air temperatures from fossil chironomid assemblages in northern Fennoscandia. The Holocene 9, 279–
669 294. doi:10.1191/095968399677918040

670 Oldfield, F., Steffen, W., 2014. Anthropogenic climate change and the nature of Earth System science. Anthr.
671 Rev. 1, 70–75. doi:10.1177/2053019613514862

672 Pinder, L.C.V., 1986. Biology of freshwater Chironomidae. Annu. Rev. Entomol. 31, 1–23.

673 Polissar, P.J., Abbott, M.B., Wolfe, a P., Bezada, M., Rull, V., Bradley, R.S., 2006. Solar modulation of Little Ice
674 Age climate in the tropical Andes. Proc. Natl. Acad. Sci. U. S. A. 103, 8937–42.
675 doi:10.1073/pnas.0603118103

676 Prat, N., Rieradevall, M., Acosta, R., Villamarín, C., M, G.D.I.F.E., 2011. Las Larvas de Chironomidae (Diptera) DE
677 Los rios Altoandinos de Ecuador y Peru, Clave par la determinacion de los generos.

678 Quinlan, R., Smol, J., 2001. Setting minimum head capsule abundance and taxa deletion criteria in chironomid-
679 based inference models. J. Paleolimnol. 26, 327–342.

680 Rees, A.B.H., Cwynar, L.C., Cranston, P.S., 2008. Midges (Chironomidae, Ceratopogonidae, Chaoboridae) as a
681 temperature proxy: a training set from Tasmania, Australia. J. Paleolimnol. doi:10.1007/s10933-008-9222-

682 6

683 Reuter, J., Stott, L., Khider, D., Sinha, A., Cheng, H., Edwards, R.L., 2009. A new perspective on the hydroclimate
684 variability in northern South America during the Little Ice Age. Geophys. Res. Lett. 36, L21706.
685 doi:10.1029/2009GL041051

686 Rieradevall, M., Brooks, S., 2001. An identification guide to subfossil Tanypodinae larvae (Insecta: Diptera:
687 Chrironomidae) based on cephalic setation. J. Paleolimnol. 81–99.

688 Self, A.E., Brooks, S.J., Birks, H.J.B., Nazarova, L., Porinchu, D., Odland, A., Yang, H., Jones, V.J., 2011. The
689 distribution and abundance of chironomids in high-latitude Eurasian lakes with respect to temperature
690 and continentality: development and application of new chironomid-based climate-inference models in
691 northern Russia. Quat. Sci. Rev. 30, 1122–1141. doi:10.1016/j.quascirev.2011.01.022

692 Telford, Birks, H.J.B., 2011a. A novel method for assessing the statistical significance of quantitative
693 reconstructions inferred from biotic assemblages. Quat. Sci. Rev. 30, 1272–1278.
694 doi:10.1016/j.quascirev.2011.03.002

695 Telford, Birks, H.J.B., 2011b. Effect of uneven sampling along an environmental gradient on transfer-function
696 performance. J. Paleolimnol. 46, 99–106. doi:10.1007/s10933-011-9523-z

697 ter Braak, C.J.F., 1987. Ordination, in: Jongman, R.., ter Braak, C.J.., van Tongeren, O.F.R. (Eds.), Data Analysis in
698 Community Ecology. Pudoc, Wageningen, The Netherlands, pp. 91–173.

699 ter Braak, C.J.F., Juggins, S., 1993. Weighted averaging partial least squares regression (WA-PLS): an improved
700 method for reconstructing environmental variables from species assemblages. Hydrobiologia 269/70, 485–
701 502.

702 ter Braak, C.J.F., Looman, C.W.., 1986. Weighted averaging, logisitc regression and the Gaussian response
703 model. Vegetatio 65, 3–11.

704 Thompson, L.., Mosley-Thompson, E., Dansgaard, W., Grootes, P.., 1986. The Little Ice Age as Recorded in the
705 Stratigraphy of the Tropical Quelccaya Ice Cap. Science. 234, 361–364.

706 Thompson, L.G., Mosley-Thompson, E., Brecher, H., Davis, M., León, B., Les, D., Lin, P.-N., Mashiotta, T.,
707 Mountain, K., 2006. Abrupt tropical climate change: past and present. Proc. Natl. Acad. Sci. U. S. A. 103,
708 10536–43. doi:10.1073/pnas.0603900103

709 Thompson, L.G., Mosley-Thompson, E., Davis, M.E., 1995. Late glacial stage and Holocene tropical ice core
710 records from Huascaran, Peru. Science. 269, 46–50.

711 Thompson, L.G., Mosley-Thompson, E., Davis, M.E., Henderson, K.A., Brecher, H.H., Zagorodnov, V.S.,
712 Mashiotta, T.A., Lin, P.-N., Mikhalenko, V.N., Hardy, D.R., Beer, J., 2002. Kilimanjaro ice core records:
713 evidence of Holocene climate change in tropical Africa. Science 298, 589–93. doi:10.1126/science.1073198

714 Trivinho-Strixino, S., 2011. Larvas de Chironomidae guia de Identificacao. Universidade Federale de Sao Carlos.

715 van Geel, B., Raspopov, O.M., Renssen, H., Plicht, J. Van Der, Dergachev, V.A., Meijer, H.A.J., 1999. The role of
716 solar forcing upon climate change. Quat. Sci. Rev. 18, 331–338.

717 Velle, G., Brodersen, K.P., Birks, H.J.B., Willassen, E., 2010. Midges as quantitative temperature indicator
718 species: Lessons for palaeoecology. The Holocene 20, 989–1002. doi:10.1177/0959683610365933

719 Velle, G., Brooks, S.J., Birks, H.J.B., Willassen, E., 2005. Chironomids as a tool for inferring Holocene climate: an
720 assessment based on six sites in southern Scandinavia. Quat. Sci. Rev. 24, 1429–1462.
721 doi:10.1016/j.quascirev.2004.10.010

722 Vuille, M., Bradley, R., Keimig, F., 2000. Climate variability in the Andes of Ecuador and its relation to tropical
723 Pacific and Atlantic sea surface temperature anomalies. J. Clim. 13, 2520–2535.

724 Walker, I.R., Cwynar, L.C., 2006. Midges and palaeotemperature reconstruction—the North American
725 experience. Quat. Sci. Rev. 25, 1911–1925. doi:10.1016/j.quascirev.2006.01.014

726 Walker, I.R., Mathews, R.W., 1987. Chironomids, lake trophic status and climate. Quat. Res. 28, 431–437.

727 Wanner, H., Beer, J., Bütikofer, J., Crowley, T.J., Cubasch, U., Flückiger, J., Goosse, H., Grosjean, M., Joos, F.,

Kaplan, J.O., Küttel, M., Müller, S.A., Prentice, I.C., Solomina, O., Stocker, T.F., Tarasov, P., Wagner, M., Widmann, M., 2008. Mid- to Late Holocene climate change: an overview. Quat. Sci. Rev. 27, 1791–1828. doi:10.1016/j.quascirev.2008.06.013

Wiederholm, T., 1983. Chironomid of the Holarctic region. Keys and diagnosis. Part 1. Larvae. Entomologica Scandinavica Supplement 19.

Woodward, C., Shulmeister, J., 2006. New Zealand chironomids as proxies for human-induced and natural environmental change: transfer functions for temperature and lake production (chlorophyll a). J. Paleolimnol. 36, 407–429.

Wu, J., Porinchu, D.F., Horn, S.P., Haberyan, K. a., 2014. The modern distribution of chironomid sub-fossils (Insecta: Diptera) in Costa Rica and the development of a regional chironomid-based temperature inference model. Hydrobiologia 742, 107–127. doi:10.1007/s10750-014-1970-x

Table captions

Table 1

Summary of the physical and chemical properties of the 59 calibration data set lakes including the total number of head capsules retrieved from each lake and the concentration of head capsules per gram of sediment. MAT= mean annual temperature, MAP= mean annual precipitation, LOI=loss-on-ignition (550°C).

Table 2

AMS radiocarbon dates used for the age-depth model of Lake Pindo. SUERC: lab code (from NERC Radiocarbon Facility, East Kilbride); BS: Bulk sediment; W: Wood; WA: weighted average.

Table 3

Results of detrended canonical correspondence analysis (DCCA) using single constraining variables. MAT= mean annual temperature, WT=water temperature, MAP=mean annual precipitation, LOI= Loss-on-ignition.

Table 4

Summary of the performance statistics of chironomid-based MAT(°C) inference models developed using classical and Bayesian methods based on leave one out cross validation. Weighted averaging inverse and classical (WAinv, WAcla), Weighted averaging partial least squares (WA-PLS), coefficient of determinant between predicted and observed (r^2_{jack}), root mean squared error of prediction ($RMSEP_{jack}$) as % of the gradient.

Tables

Table 1

	Calibration data set				
	Minimum	**Mean**	**Median**	**Maximum**	**Std dev**
Conductivity (µs)	5.9	363	185	3205	579
Depth (m)	0.1	5	2.2	25	5.4
Elevation (m a.s.l)	150	3142	3845	4655	1459
Latitude (S)	0.1	11.2	14.2	17.3	6.2
Longitude (W)	64.4	71.6	70.3	78.4	4.5
LOI (%)	0	19	13	80	16
MAT (°C)	0.8	12	10	25	7
MAP (mm/year)	468	1222	769	4421	952
pH	5.7	8	7.9	10.2	1.1
Total Head Capsules	23	77	76	164	35
Water Temperature (°C)	5	15	13	33	6
Head capsule/gram	2	27	22	105	22

Table 2

Sample code	Depth (cm)	Sample type	Age (yr ^{14}C BP)	Age (cal yrs BP) 2σ	Age (cal yr BP) estimation (WA)
SUERC- 54395	46	W	334 ± 42	289-470	373
SUERC-47634	117	W	974 ± 36	769-923	835
SUERC-47635	245	W	1973 ± 39	1812-1943	1868
SUERC-47569	329	W	2335 ± 37	2293-2361	2279
SUERC-47572	410	W	2829 ± 39	2781-2991	2916
SUERC-48854	461	BS	3974 ± 45	4241-4447	4336

Table 3

Variable	Variance Explained (%)	λ_1/λ_2	*P*
MAT	12.93	1.431	0.001
MAP	10.3	0.900	0.001
WT	11.21	1.230	0.001
pH	6.23	0.500	0.001
LOI	3.23	0.239	0.062
Depth	2.44	0.190	0.240
Conductivity	2.34	0.179	0.296

Table 4

Model	R^2_{Jack}	$RMSEP_{jack}$	Mean $bias_{jack}$	Max $bias_{jack}$	% change
WA (inv)	0.890	2.404	-0.017	4.665	-
WA (cla)	0.890	2.475	-0.035	4.279	-2.936
WA-TOL (inv)	0.851	2.831	-0.182	6.498	-
WA-TOL (cla)	0.852	2.951	-0.211	7.350	-4.263
WA-PLS (1)	0.889	2.431	0.094	4.891	-
WA-PLS (2)	0.890	2.412	0.109	3.982	0.766
WA-PLS (3)	0.869	2.617	0.096	5.558	-8.483
WA-PLS (4)	0.866	2.659	0.199	5.922	-1.592
WA-PLS (5)	0.875	2.568	0.213	6.201	3.409
Bayesian	0.909	2.373	0.598	3.158	

817 **Figure captions**

818 **Figure 1**

819 Location of the calibration data set lakes (black circles) and Laguna Pindo (white triangle).

820 Figure 2

821 Sediment description, radiocarbon dates (^{14}C age) and age-depth models of Laguna Pindo. Key colour for
822 sediment descriptions: Black or dark brown = organic rich sediments (peat and clay respectively); White = dark
823 sandy intervals; Greenish =greenish sandy clay, not compacted; Yellow = sediment gap (no sediment).

824 **Figure 3**

825 Figure 2: Canonical correspondence analysis (CCA) of the calibration data set lakes and environmental variables
826 with elevation and longitude removed after variance inflation analysis. MAP=mean annual precipitation,
827 MAT=mean annual temperature, WT= water temperature, LOI=loss-on-ignition. Grey circles denote calibration
828 lakes, dark grey triangles mark species. All species could not be labelled due to crowding; instead nine
829 important taxa have been marked as examples.

830 **Figure 4**

831 Chironomid taxa in the modern calibration dataset lakes. Lakes are ordered (top to bottom) from cold to warm
832 and chironomids are ordered by occurrence from cold to warm lakes. Only taxa present in three or more lakes
833 are included. Dashed line shows a gap in calibration data set lakes between 16-20 °C of the MAT gradient.
834 Detrended canonical correspondence analysis (DCCA) constrained by MAT shows the taxon turnover across the
835 gradient. Head capsule concentration (hc/gram) is also included.

836 **Figure 5**

837 Weighted-average and Bayesian optima (*solid grey circles*) and tolerances (*thick lines*) of the 55-chironomid taxa
838 included in the calibration dataset, MAT Range (*dashed lines*). Taxa are organised by WA temperature optima
839 from cold to warm.

840 **Figure 6**

Model performance of the best performing classical method (WA) and Bayesian approach. A=weighted averaging method; B=Bayesian method. WA: R^2_{jack}= 0.890, $RMSEP_{jack}$ = 2.404°C, Mean $bias_{jack}$= -0.017°C, Max $bias_{jack}$=4.665°C. Bayesian: R^2_{jack}= 0.909, $RMSEP_{jack}$ =2.373°C, Mean $bias_{jack}$= 0.598°C, Max $bias_{jack}$= 3.158°C.

Figure 7

Diagram of fossil chironomid assemblage of Laguna Pindo. Five significant zones were identified using optimal partitioning with a broken stick model. Detrended canonical correspondence analysis (DCCA) constrained by calibrated radiocarbon age shows taxon turnover through time. Only taxa with relative abundances greater than 5% are shown. SD=standard deviation, hc/gram= head capsules per gram of wet sediment.

Figure 8

Chironomid-inferred mean annual temperatures (MAT) at Laguna Pindo using the WA inverse (grey) and Bayesian (black) models. Sample specific errors for the WA model are obtained through bootstrapping 999 cycles. Errors of the Bayesian reconstruction are site-specific uncertainties.

Figure 9

Distribution of Laguna Pindo fossil samples (black circles) included passively within a CCA of the calibration data set lakes (grey circles) constrained using the significant environmental variables. MAP= mean annual precipitation, MAT= mean annual temperature, WT= water temperature. The first and last fossil sample in the sedimentary sequence has been labelled (total sediment depth); there are no directional trends through time. Calibration lakes that lie at similar elevations as Laguna Pindo have been labelled.

Figure 10

(left to right): Chironomid-inferred WA classical MAT with sample specific errors generated using bootstrapping. Bayesian reconstruction with sample specific errors. Goodness-of-fit of the fossil assemblages to temperature, vertical dotted line indicates the 90^{th} percentile of squared residual distances of modern samples to first axis in a CCA; samples to the right of the line have a poor fit-to-temperature. Nearest modern analogue analysis, vertical dotted line indicates the 5^{th} percentile of squared chord distances of the fossil samples in the modern calibration data set; samples to the right of the line have no good modern analogues. Detrended canonical

correspondence analysis (DCCA) sample scores with radiocarbon age used as the sole constraining variable. Head capsule concentration per gram of sediment. Zones are derived from optimal partitioning of fossil assemblages using a broken stick model to define significant zones. Sq res dis= square residual distance; Sq chrd dis= square chord distance; SD units= standard deviation units; hc/gram=head capsule per gram of sediment.

Figure 11

Histogram of the proportion of variance in the chironomid MAT transfer function explained by 999 transfer functions trained on random environmental variables. Solid black line denotes the proportion of variance explained by the chironomid WA inverse MAT transfer function. Black dashed line marks the proportion of variance explained by the first axis of PCA of the fossil data. Grey dashed line marks the 95% variance of the random reconstructions.

Figure 12

Individual likelihood functions for the fossil taxa in the coldest sample of the Laguna Pindo sequence (396 cm total depth, *c.* 2700 cal yr BP). The posterior probability distribution for temperature for the fossil sample is plotted in red, note this is plotted on an independent axis.

Figures

Figure 1

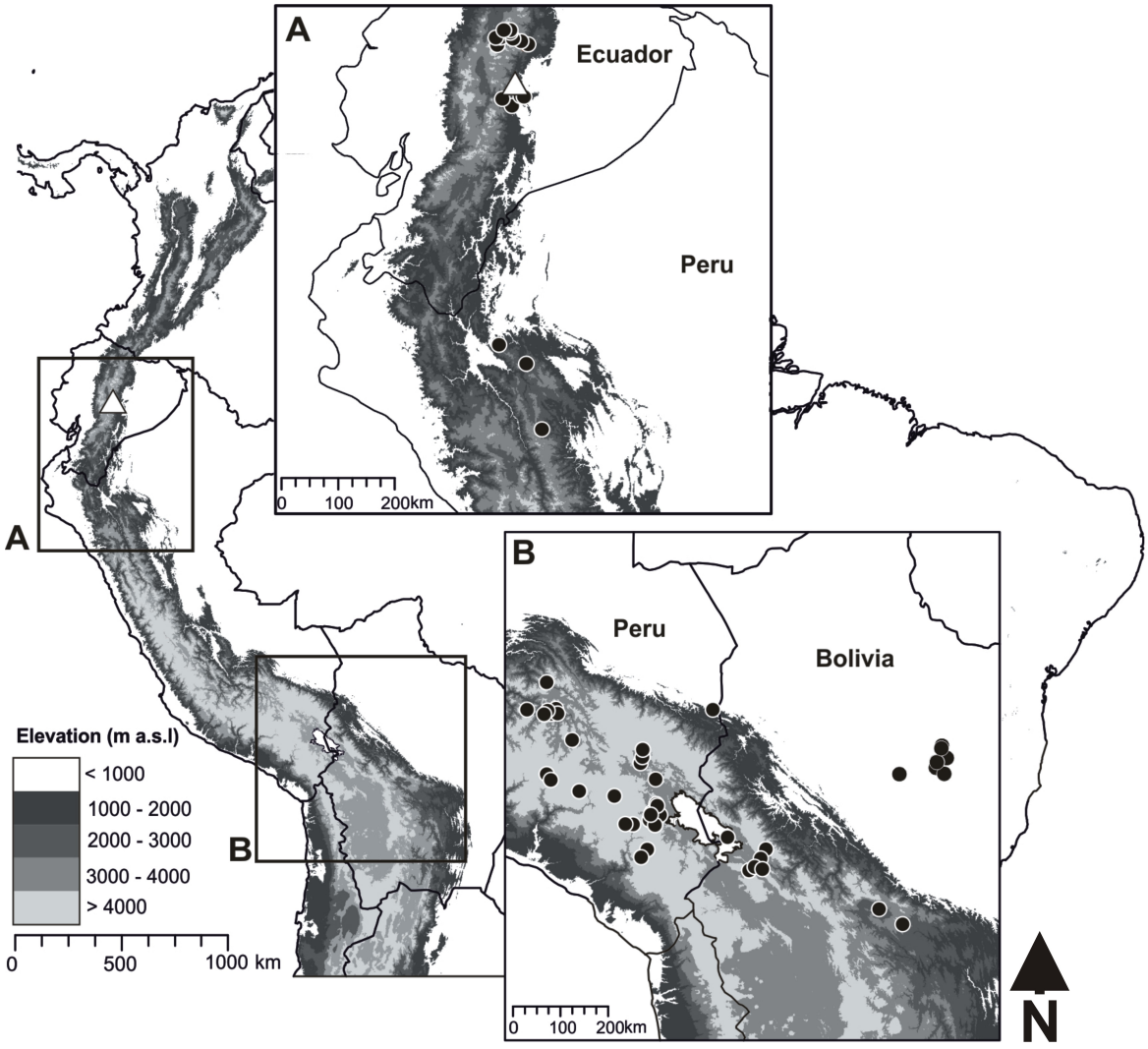

Figure 2

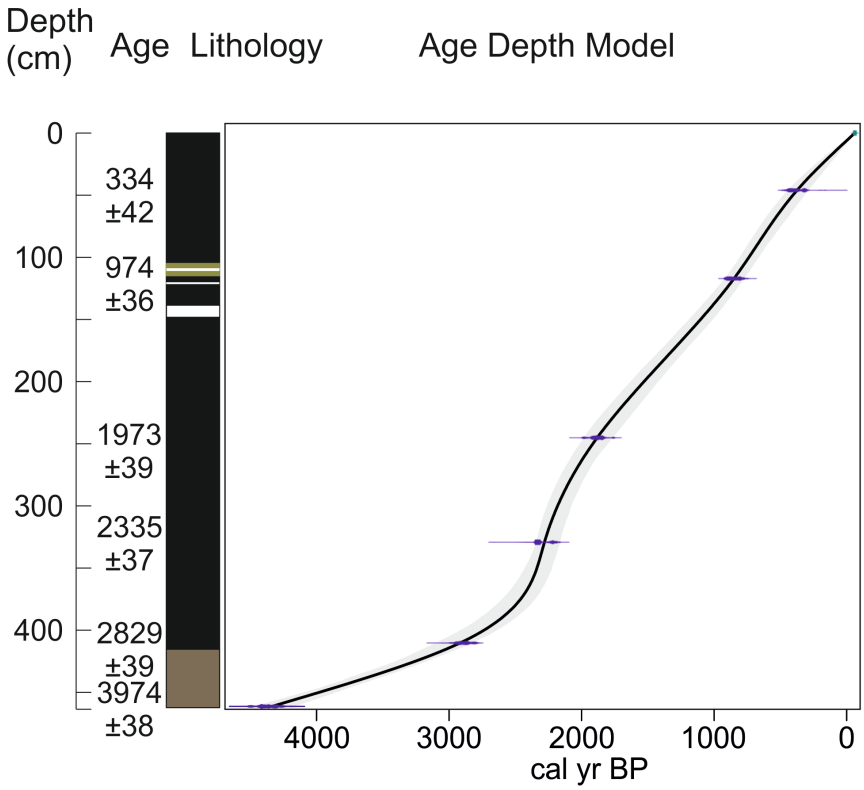
Depth (cm)
Age
Lithology
Age Depth Model
0
100
200
300
400
334 ±42
974 ±36
1973 ±39
2335 ±37
2829 ±39
3974 ±38
4000
3000
2000
1000
0
cal yr BP

Figure 3

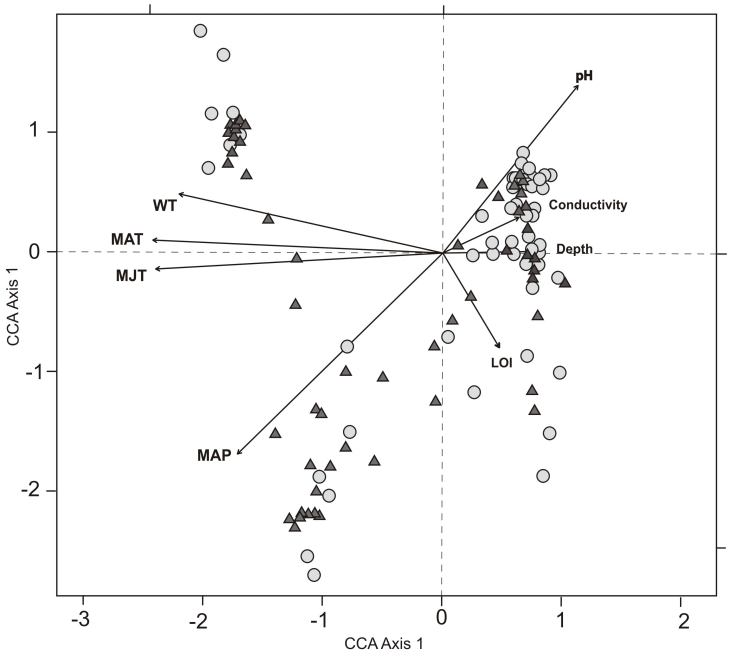
pH
Conductivity
Depth
LOI
MAP
WT
MAT
MJT
CCA Axis 1
CCA Axis 1
1
0
-1
-2
-3
-2
-1
0
1
2

Figure 4

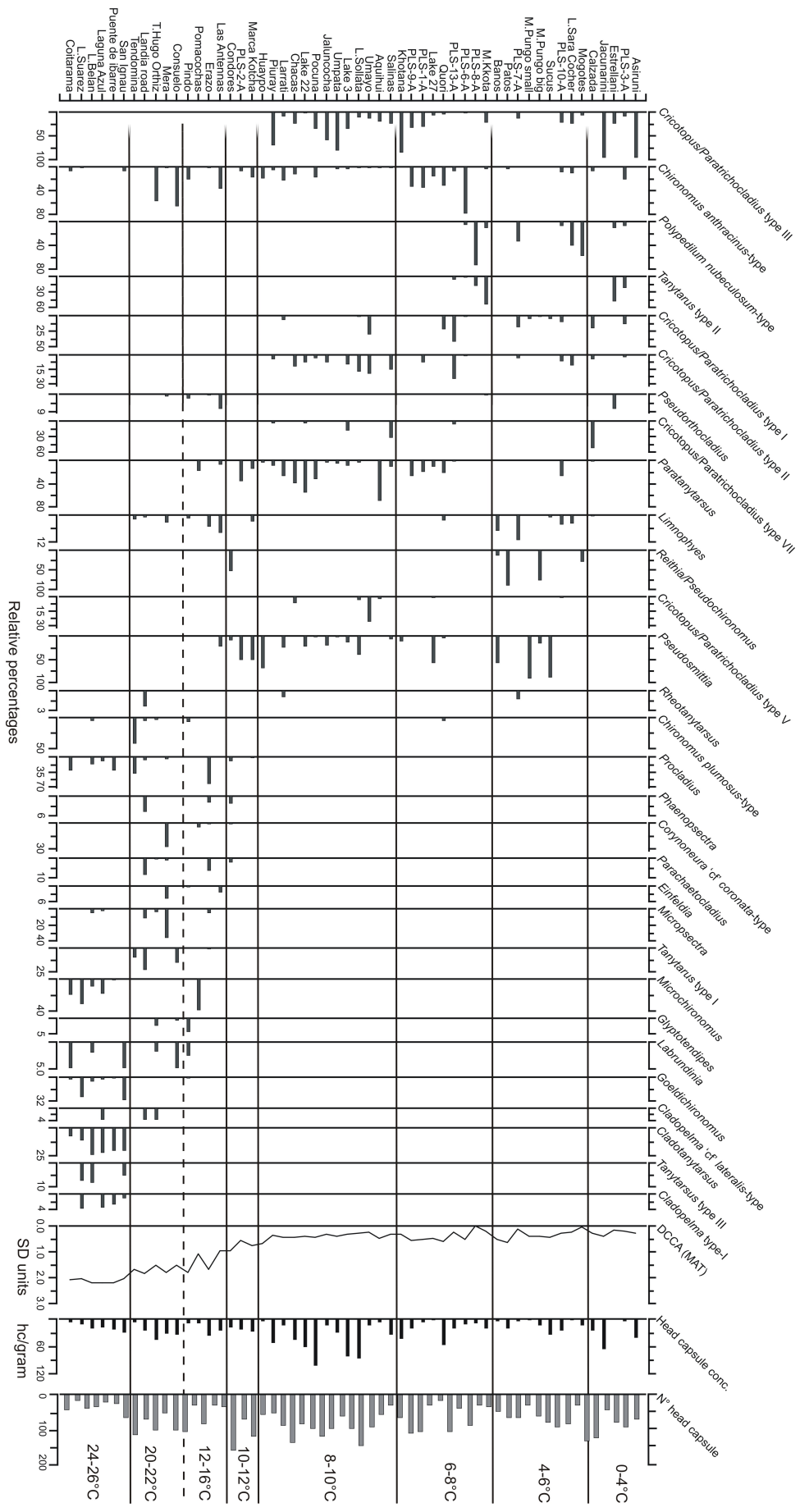
Asiruni
PLS-3-A
Estrellani
Jacunarini
Calzada
Mogotes
L.Sara Cocher
PLS-10-A
S-10-A
M.Pungo big
M.Pungo small
PLS-7-A
Patos
Banos
M.Kkota
PLS-8-A
PLS-6-A
PLS-13-A
Quon
Lake 27
PLS-1-A
PLS-5-A
Kkota-A
Salinas
Aquihui
Umayo
L.Solata
Lake 3
Umpata
Jaluncocha
Pocuna
Lake 22
Chacas
Larrati
Pluray
Huaypo
Marca Kkota
PLS-2-A
Condores
Las Antennas
Erazo
Pomacochas
Pindo
Consuelo
Mera
T.Hugo Orthiz
Landia road
Tendomina
San Ignau
Puente de Ibarre
Laguna Azul
L.Suarez
Coitarama
Cricotopus/Paratrichocladius type III
Chironomus anthracinus-type
Polypedilum nubeculosum-type
Tanytarus type II
Cricotopus/Paratrichocladius type I
Cricotopus/Paratrichocladius type II
Pseudorthocladius
Cricotopus/Paratrichocladius type VII
Paratanytarsus
Limnophyes
Reithia/Pseudochironomus
Cricotopus/Paratrichocladius type V
Pseudosmittia
Rheotanytarsus
Chironomus plumosus-type
Procladius
Phaenopsectra
Corynoneura 'cf' coronata-type
Parachaetocladius
Einfeldia
Micropsectra
Tanytarus type I
Microchironomus
Glyptotendipes
Labrundinia
Goeldichironomus
Cladopelma 'cf' lateralis-type
Cladotanytarsus
Tanytarsus type III
Cladopelma type-I
DCCA (MAT)
Head capsule conc.
N° head capsule
Relative percentages
SD units
hc/gram
24-26°C
20-22°C
12-16°C
10-12°C
8-10°C
6-8°C
4-6°C
0-4°C

Figure 5

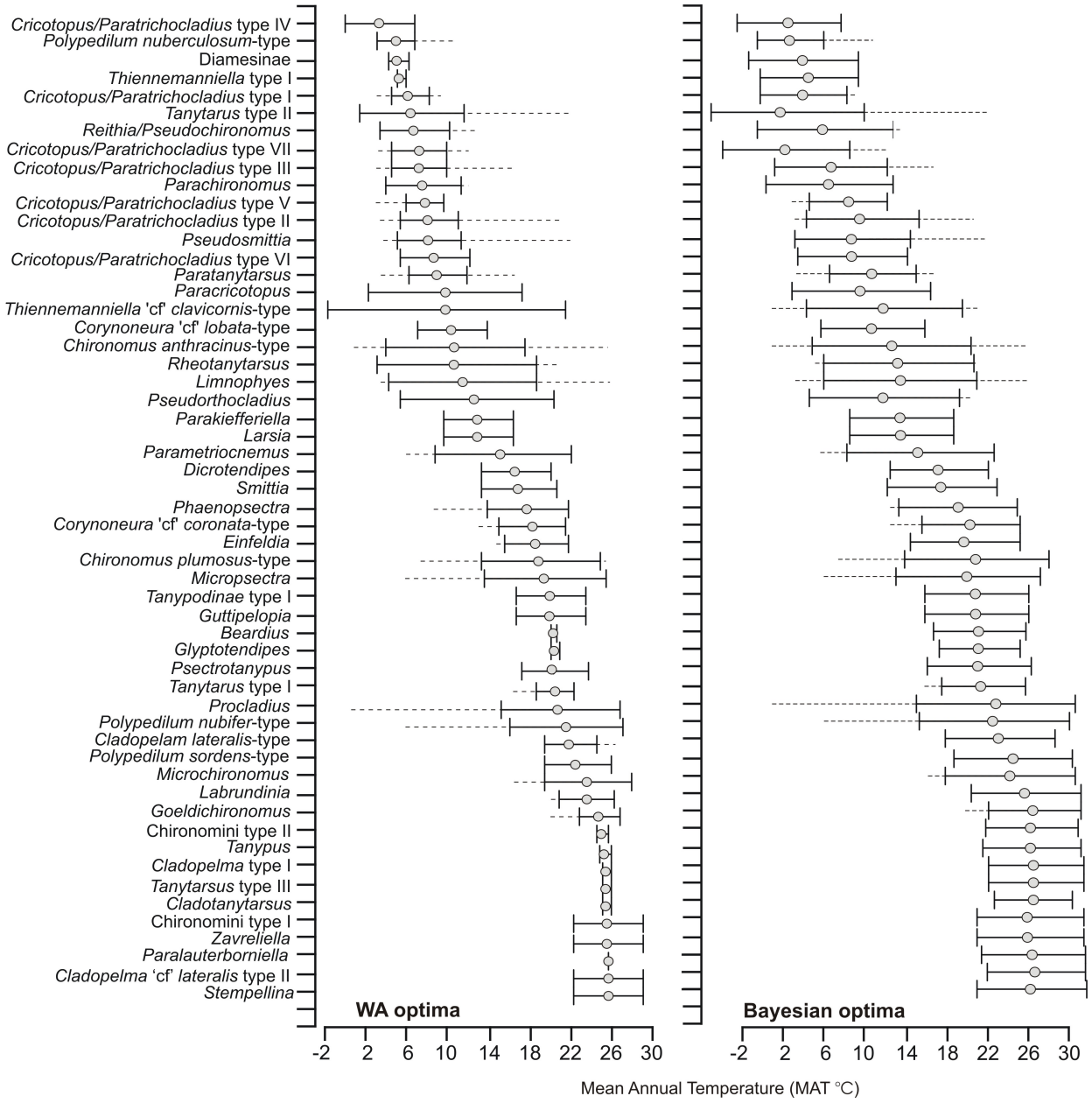
Cricotopus/Paratrichocladius type IV
Polypedilum nuberculosum-type
Diamesinae
Thiennemanniella type I
Cricotopus/Paratrichocladius type I
Tanytarus type II
Reithia/Pseudochironomus
Cricotopus/Paratrichocladius type VII
Cricotopus/Paratrichocladius type III
Parachironomus
Cricotopus/Paratrichocladius type V
Cricotopus/Paratrichocladius type II
Pseudosmittia
Cricotopus/Paratrichocladius type VI
Paratanytarsus
Paracricotopus
Thiennemanniella 'cf' clavicornis-type
Corynoneura 'cf' lobata-type
Chironomus anthracinus-type
Rheotanytarsus
Limnophyes
Pseudorthocladius
Parakiefferiella
Larsia
Parametriocnemus
Dicrotendipes
Smittia
Phaenopsectra
Corynoneura 'cf' coronata-type
Einfeldia
Chironomus plumosus-type
Micropsectra
Tanypodinae type I
Guttipelopia
Beardius
Glyptotendipes
Psectrotanypus
Tanytarus type I
Procladius
Polypedilum nubifer-type
Cladopelam lateralis-type
Polypedilum sordens-type
Microchironomus
Labrundinia
Goeldichironomus
Chironomini type II
Tanypus
Cladopelma type I
Tanytarsus type III
Cladotanytarsus
Chironomini type I
Zavreliella
Paralauterborniella
Cladopelma 'cf' lateralis type II
Stempellina
WA optima
Bayesian optima
-2 2 6 10 14 18 22 26 30
-2 2 6 10 14 18 22 26 30
Mean Annual Temperature (MAT °C)

Figure 6

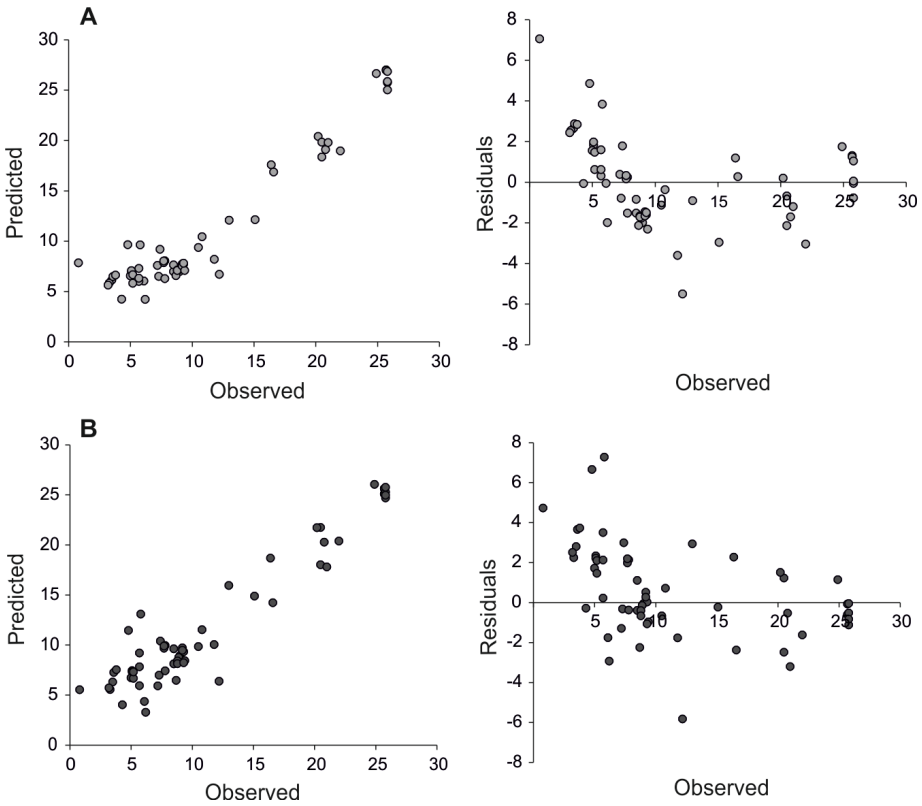
A
Predicted
Observed
Residuals
Observed
B
Predicted
Observed
Residuals
Observed

Figure 7

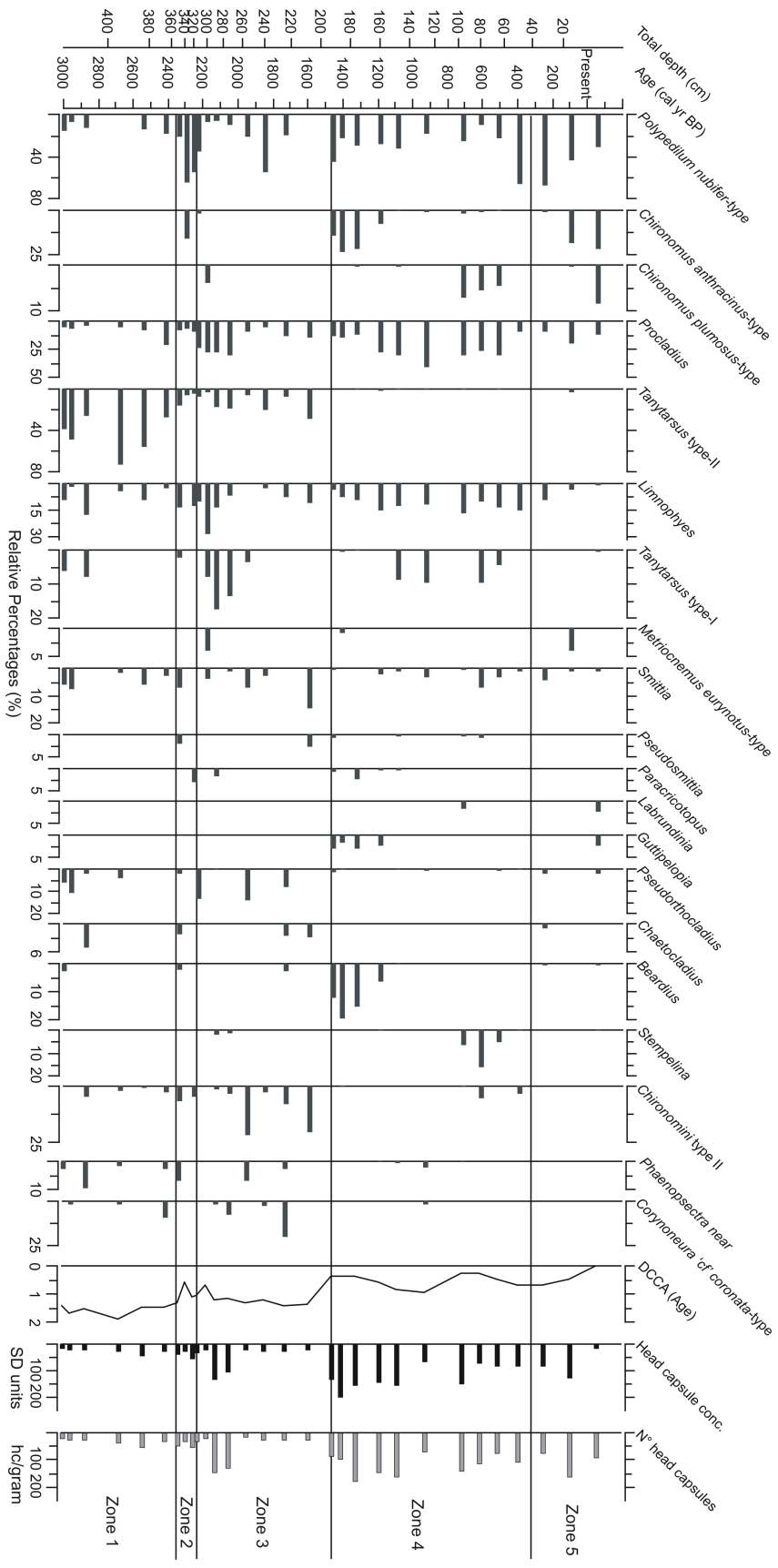
Total depth (cm)
Age (cal yr BP)
Present
Relative Percentages (%)
Polypedilum nubifer-type
Chironomus anthracinus-type
Chironomus plumosus-type
Procladius
Tanytarsus type-II
Limnophyes
Tanytarsus type-I
Metriocnemus eurynotus-type
Smittia
Pseudosmittia
Paracricotopus
Labrundinia
Guttipelopia
Pseudorthocladius
Chaetocladius
Beardius
Stempellina
Chironomini type II
Phaenopsectra near
Corynoneura 'cf coronata-type
DCCA (Age)
Head capsule conc.
SD units
N° head capsules
hc/gram
Zone 1
Zone 2
Zone 3
Zone 4
Zone 5

Figure 8

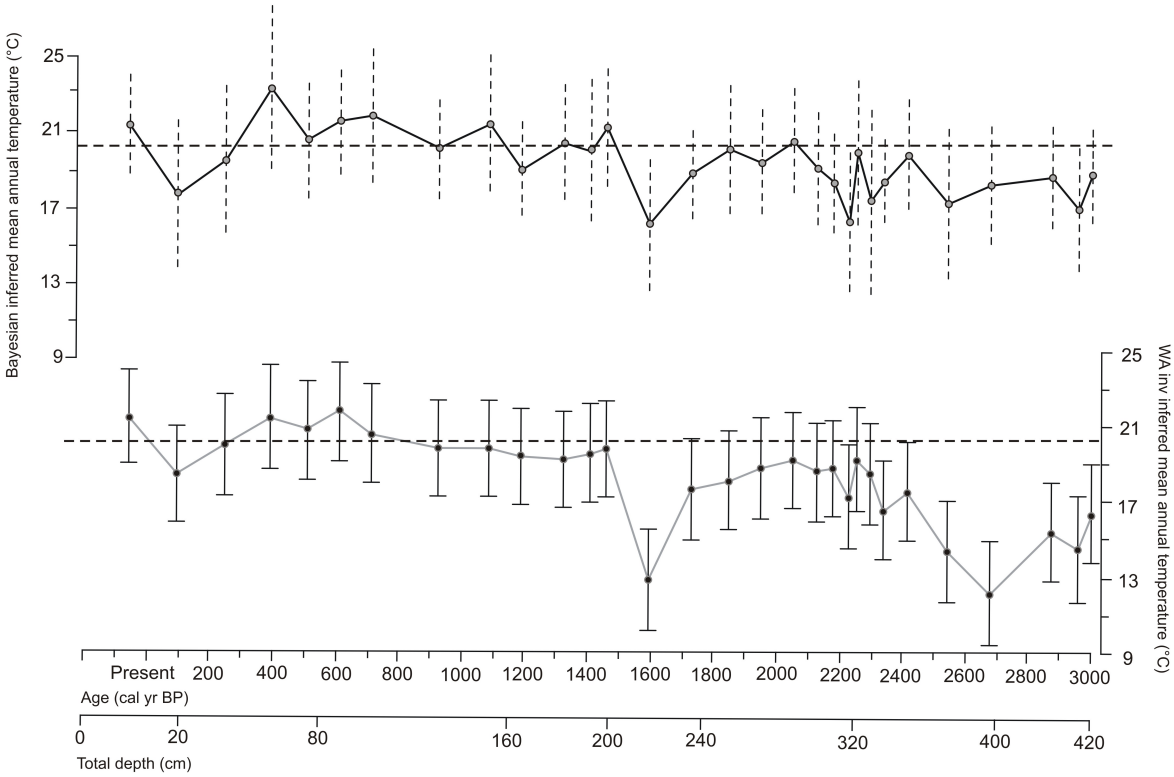
Bayesian inferred mean annual temperature (°C)
25
21
17
13
9
WA inv inferred mean annual temperature (°C)
Present
200
400
600
800
1000
1200
1400
1600
1800
2000
2200
2400
2600
2800
3000
Age (cal yr BP)
0
20
80
160
200
240
320
400
420
Total depth (cm)

Figure 9

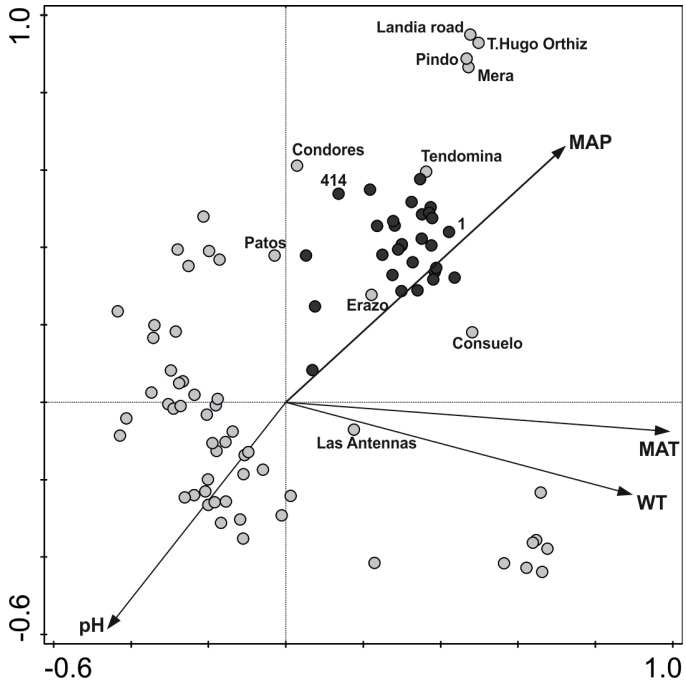
Landia road
T.Hugo Orthiz
Pindo
Mera
Condores
Tendomina
414
MAP
1
Patos
Erazo
Consuelo
Las Antennas
MAT
WT
pH
1.0
-0.6
-0.6
1.0

Figure 10

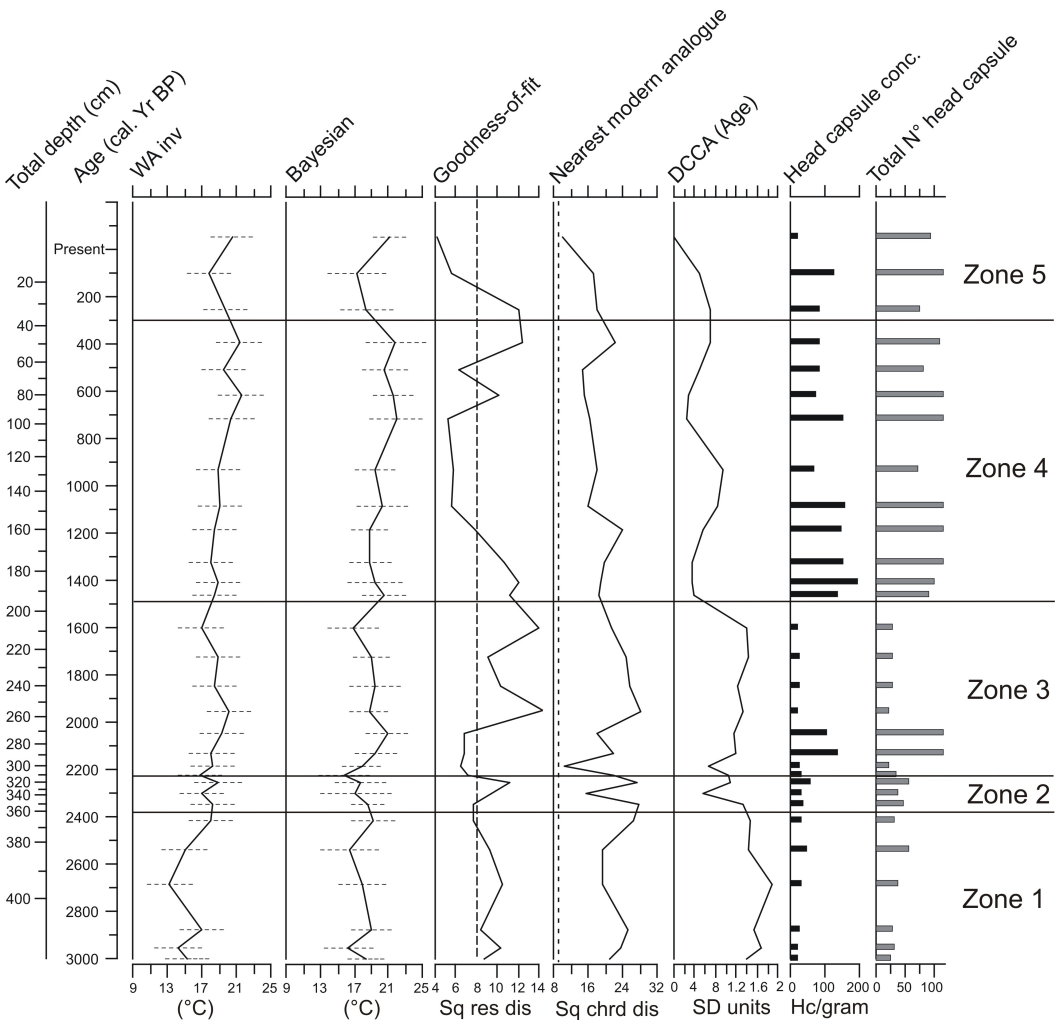
Total depth (cm)
Age (cal. Yr BP)
WA inv
Bayesian
Goodness-of-fit
Nearest modern analogue
DCCA (Age)
Head capsule conc.
Total N° head capsule
Present
Zone 5
Zone 4
Zone 3
Zone 2
Zone 1
(°C)
(°C)
Sq res dis
Sq chrd dis
SD units
Hc/gram

Figure 11

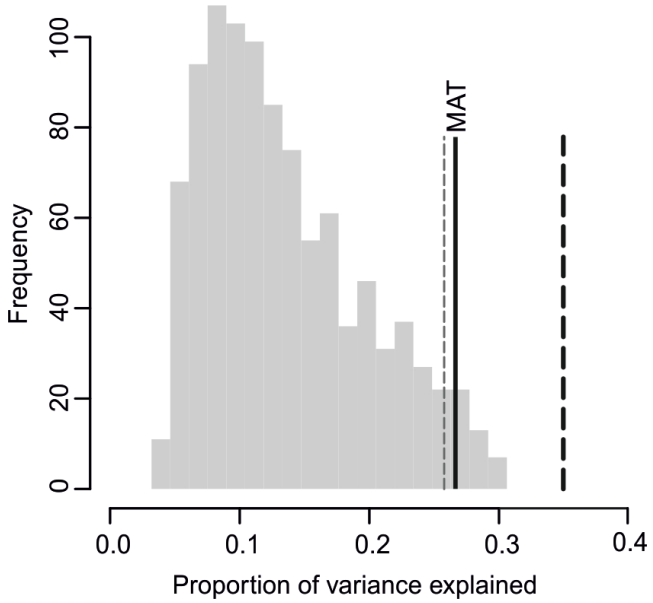
Frequency
0
20
40
60
80
100
MAT
0.0
0.1
0.2
0.3
0.4
Proportion of variance explained

Figure 12

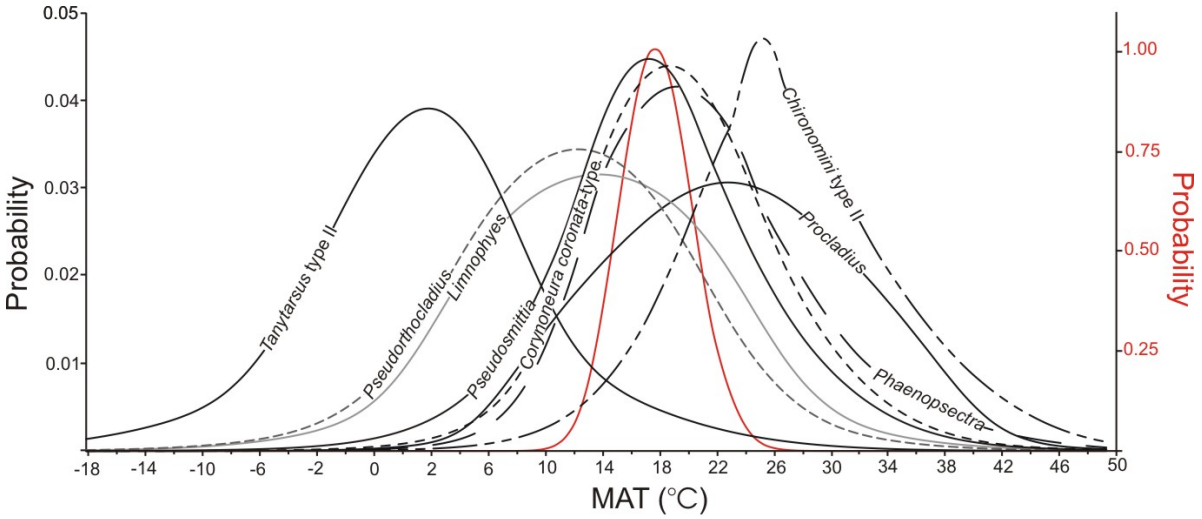
Probability
0.05
0.04
0.03
0.02
0.01
1.00
0.75
0.50
0.25
Probability
Tanytarsus type II
Pseudorthocladius
Limnophyes
Pseudosmittia
Corynoneura coronata-type
Chironomini type II
Procladius
Phaenopsectra
-18 -14 -10 -6 -2 0 2 6 10 14 18 22 26 30 34 38 42 46 50
MAT (°C)